


Physicochemical hydrodynamics of droplets out of equilibrium

Detlef Lohse  and Xuehua Zhang

Abstract | Droplets abound in nature and technology. In general, they are multicomponent, and, when out of equilibrium, have gradients in concentration, implying flow and mass transport. Moreover, phase transitions can occur, in the form of evaporation, solidification, dissolution or nucleation of a new phase. The droplets and their surrounding liquid can be binary, ternary or contain even more components, with several in different phases. Since the early 2000s, rapid advances in experimental and numerical fluid dynamical techniques have enabled major progress in our understanding of the physicochemical hydrodynamics of such droplets, further narrowing the gap from fluid dynamics to chemical engineering and colloid and interfacial science, arriving at a quantitative understanding of multicomponent and multiphase droplet systems far from equilibrium, and aiming towards a one-to-one comparison between experiments and theory or numerics. This Perspective discusses examples of the physicochemical hydrodynamics of droplet systems far from equilibrium and the relevance of such systems for applications.

Classical hydrodynamics focuses on pure liquids. However, in nature and technology, many fluid dynamical systems are multicomponent, and often have gradients in concentration, even changing in time: that is, they are out of equilibrium. These concentration gradients, whether smooth or sharp, can induce a flow. Moreover, phase transitions can occur, with evaporation, solidification, dissolution or nucleation of a new phase. The liquids can be binary, ternary or contain even more components, with several across different phases. The non-equilibrium nature can be driven by processes such as flow, mixing, phase transitions, chemical reactions, electrical current or heat supply.

To deal with such systems theoretically, in the 1950s Veniamin Grigor'evich Levich wrote the wonderful book *Physicochemical Hydrodynamics*¹. The central theme of the book is the “elucidation of mechanisms of transport phenomena and the conversion of understanding so gained into plain, useful tools for applications,” as Laurence E. Scriven describes it in the foreword to the book in its 1962 translation into English¹. Levich can be viewed as a physical chemist and theoretical

physicist at the same time, or, as Scriven puts it, above all, as an ‘engineering scientist’ with a recognizable “blend of applied chemistry, applied physics, and fluid mechanics”. Levich himself, in his foreword to the first Russian edition (1952), describes the scope of physicochemical hydrodynamics as the “aggregate of problems dealing with the effect of fluid flow on chemicals or physicochemical transformations as well as the effect of physicochemical factors of the flow”.

First and foremost, Levich's *Physicochemical Hydrodynamics* is a book describing the relevant theoretical and mathematical concepts. When it was written, the experimental tools to measure flow on the microscale were limited, and there was no possibility of performing direct numerical simulations of the underlying partial differential equations. Today, more than 60 years later, the scientific (and in particular the hydrodynamical and physicochemical) communities have developed tremendously, and the experimental, instrumental and numerical means to deal with the problems that Levich defined in his book have become available and are being put to use.

These developments are timely, as the relevance of physicochemical hydrodynamics of multicomponent and multiphase liquids is ever-increasing, to address the challenges of humanity for the twenty-first century. These challenges include energy — namely storage and batteries, hydrogen production by electrolysis, CO₂ capture, polymeric solar cell manufacturing, biofuel production, and catalysis. They also include health and medical issues such as chemical analysis and diagnostics or the production and purification of drugs; advanced material manufacturing; environmental issues such as flotation, water cleaning, membrane management and separation technology; and food processing and food safety issues. In modern production technologies, challenges include additive manufacturing on ever-decreasing length scales, inkjet printing, and issues in the paint and coating industry.

These challenges have often been approached with a pure engineering approach, and less in the spirit of Levich as an engineering scientist. On the other hand, as already mentioned, classical hydrodynamics has focused on pure and single-phase liquids. Since the early 2000s, the advent of new experimental and numerical tools has allowed for a more integrated understanding of physicochemical hydrodynamics and a further narrowing of the gap between classical hydrodynamics and chemical engineering and colloid and interfacial science. The objective of this effort is to improve the quantitative understanding of multicomponent and multiphase fluid dynamic systems far from equilibrium, to master and better control them. To achieve this, one must perform controlled experiments and numerical simulations for idealized set-ups, allowing one-to-one comparison between experiments and numerics and/or theory, to test the theoretical understanding. This effort is in the spirit of Levich's *Physicochemical Hydrodynamics*, but now building on and benefiting from the developments of modern microfluidics, microfabrication, digital (high-speed) imaging technology, confocal microscopy, atomic force microscopy, and various computational techniques and opportunities

for high-performance computing. These methods are the blessings of a golden age of fluid dynamics, which builds on the digital revolution, both on the experimental and the numerical side. Given these developments, and given the need in chemical engineering to move towards increased precision and control, this effort is timely.

Many physical phenomena and effects come into play in multicomponent and multiphase liquids far from equilibrium.

For the control and driving parameters, we refer to BOX 1 and for the experimental and numerical tools to BOXES 2 and 3, respectively. The physical phenomena and effects that come into play include gradients in concentration, whether in the bulk of the liquid or on the surface, which lead to diffusiophoresis and solutal Marangoni flow, either at the interface of a droplet immersed in another liquid (FIG. 1) or when two droplets of different

liquids touch (FIG. 2). Effects also include (possibly selective) dissolution of (possibly multicomponent) droplets in host liquids (FIG. 3) or selective evaporation of droplets in air (FIG. 4), or, vice versa, droplet nucleation and growth. Other effects include the coalescence of droplets consisting of different liquids with chemical reactions and/or solidification and other transitions from one phase to another (FIGS 5,6,7). The material parameters that become important are the various diffusivities and viscosities of the liquids, their surface tensions and how they depend on the concentrations, the volatilities and mutual solubilities, latent heats and reaction rates, among others.

The field of multicomponent and multiphase hydrodynamics is too large to give an exhaustive review. This Perspective is restricted to small length scales, focusing on the physicochemical hydrodynamics of (possibly multicomponent) droplets far from equilibrium. The objectives of this Perspective are to show examples of such systems for which a successful quantitative description and one-to-one comparison between well-controlled table-top experiments and theory and numerics have been achieved; to identify the complex interplay of the underlying principles; and to put these examples into the context of relevant applications of multicomponent and multiphase liquid systems. In particular, we aim to identify the new directions of physicochemical hydrodynamics and outline the scientific challenges and their connections with the technological challenges mentioned above.

This Perspective discusses various examples of the physicochemical hydrodynamics of droplet systems far from equilibrium and our present understanding of them. This section is the core of the article. Examples surveyed include immiscible droplets in a concentration gradient, coalescence of droplets of different liquids, droplets in concentration gradients emerging from chemical reactions (including droplets as microswimmers) and phase transitions such as evaporation, solidification, dissolution or nucleation, and droplets in ternary liquids, including solvent exchange, nanoprecipitation and the 'ouzo effect'. We then discuss the relevance of the physicochemical hydrodynamics of such droplet systems for many important applications, including in chemical analysis and diagnostics, microanalysis, pharmaceuticals, synthetic chemistry and biology, chemical and environmental engineering, the oil and remediation industries, inkjet printing, for micromaterials and

Box 1 | Dimensionless numbers for droplets in physicochemical hydrodynamics

In fluid dynamics, it is common to express the ratio of the various forces (or timescales or length scales) in terms of dimensionless numbers. The most famous is the

- **Reynolds number** $Re = UR/\nu$, which expresses the ratio of inertial forces to viscous forces. In the context of droplets, R is the droplet radius, U the (relative) droplet velocity and ν the kinematic viscosity of the continuous phase.

In the context of the physicochemical hydrodynamics of droplets that dissolve or grow, the perhaps even more relevant dimensionless parameter is the

- (diffusive) **Peclet number** $Pe = UR/D$, which compares the advective and diffusive timescales, where D is the mass diffusivity, which in general is much smaller than the viscosity, reflecting the slowness of the process of molecular diffusion in liquids.

The ratio between viscosity and diffusivity is the

- **Schmidt number** $Sc = \nu/D$, which correspondingly in physicochemical hydrodynamics is large, namely $\sim 10^3$. The large value of Sc on the one hand is the reason for many peculiarities in physicochemical hydrodynamics, and on the other hand introduces many experimental and numerical difficulties.

Once thermal effects also come into play, the thermal diffusivity κ has a role. Its ratio to the molecular diffusivity and the kinematic viscosity is expressed as the

- **Lewis number** $Le = \kappa/D$ and **Prandtl number** $Pr = \nu/\kappa$. Typically, Le is ~ 400 and Pr is ~ 4 , reflecting the fact that thermal diffusion is much faster than molecular diffusion, and that for standard liquids thermal transport is slightly slower than viscous transport.

In hydrochemical hydrodynamics, surface tension effects are crucial. They can be expressed in terms of the

- **Weber number** $We = \rho U^2 R/\sigma$, which is the ratio of inertia to capillarity, where σ is the surface tension and ρ the density of the liquid; or the
- **Capillary number** $Ca = \eta U/\sigma$, (where η is the dynamic viscosity), which is the ratio of viscous to capillary forces; or the
- **Ohnesorge number** $Oh = \eta/(\rho\sigma R)^{1/2} = We^{1/2}/Re$, which is the ratio of time of viscous damping to time of the capillary oscillations; or the
- **Bond number** $Bo = \rho g R^2/\sigma$, which is the ratio of gravity to capillary forces.

The full richness of hydrochemical droplet fluid dynamics only arises once several liquids and gases are part of the system under study, with different surface tensions, densities and other properties. In that case, the gradient of the hydrodynamic forces along or across a droplet introduces net forces. The most relevant may be the

- **Marangoni number** $Ma = R\Delta\sigma/(\rho\nu D)$, which compares the Marangoni forces with stabilizing viscous forces and stabilizing mass diffusion. The difference $\Delta\sigma$ in surface tension may be due to differences Δc in the composition of the liquid, where $c(x,t)$ is the concentration field, or due to differences ΔT in the temperature of the liquid. Roughly, $\Delta\sigma \approx \partial\sigma/\partial c\Delta c$, and similarly for the temperature, but note that in general the dependence $\sigma(c)$ is very nonlinear¹⁹⁵. In general, σ is a function of both c and T , and $\Delta\sigma \approx \partial_r\sigma|_c\Delta T + \partial_c\sigma|_T\Delta c$.

Another way for the system to get out of equilibrium is density differences $\Delta\rho$ to which the gravitational acceleration g couples, implying a

- **Rayleigh number** $Ra = gR^3\Delta\rho/(\rho\nu D)$, which compares destabilizing buoyancy with stabilizing viscosity and diffusivity.

If chemical reactions come into play, another necessary dimensionless number is the

- **Damköhler number** Da , which expresses the ratio between chemical reaction rate and (diffusive or convective) mass transport rate.

All these numbers appear in the discussions of the various physicochemical hydrodynamical effects featured in this Perspective.

nanomaterials, and in nanotechnology. For better readability, so that in the main sections we can focus on the fluid dynamics and the physics, we have included three text boxes: one on the relevant dimensionless numbers in physicochemical hydrodynamics (BOX 1), one for the new experimental methods that have enabled recent progress (BOX 2), and one on new or improved numerical methods (BOX 3).

This Perspective conveys ideas, rather than delving into technical details or attempting to be encyclopaedic. For these aspects, we refer to specialized review articles on certain aspects, such as binary fluid mixtures², swimmers³, swimming droplets⁴, phoretic self-propulsion^{5,6}, surfactant dynamics⁷, evaporation of pure liquid sessile droplets^{8,9}, patterns from drying drops¹⁰, surface nanobubbles and nanodroplets¹¹, single-drop microextraction¹², or chemo-hydrodynamic patterns and instabilities¹³.

Recent fundamental research

In this section, we give examples for the physicochemical hydrodynamics in selected simple droplet systems. We focus on systems in which modern experimental and numerical techniques have led to considerable progress in understanding, often even allowing for a one-to-one comparison between experiments and numerics. These modern techniques are highlighted in BOX 2 (experimental) and BOX 3 (computational). In the next section, we focus on the applications and the relevance of these examples. The focus is on droplets; for a very general overview on fundamental and applied aspect of bubble systems, we refer to our recent review¹⁴.

Immiscible droplet in a concentration gradient. One of the most basic examples of a droplet far from physicochemical equilibrium is that of an immiscible (for example, oil) droplet of radius R in a concentration gradient of two other miscible liquids, with density lower and higher than the oil droplet (FIG. 1a). The two control parameters reflecting the non-equilibrium situation are the Marangoni number Ma , which depends on the gradient of the surface tension, that is, $\Delta\sigma = R\partial_c\sigma$, and the Rayleigh number Ra , which depends on the gradient in density (ρ), $\Delta\rho = R\partial_c\rho$; see BOX 1 for the proper non-dimensionalization. For the case of Stokes flow (small Reynolds number) and zero density gradient, the resulting velocity and the concentration fields can be analytically calculated¹⁵. The former can be quantified by the

Box 2 | Experimental tools to address physicochemical hydrodynamics

A plethora of new and improved experimental techniques in fluid dynamics has enabled progress in understanding the physicochemical hydrodynamics of droplets and bubbles far from equilibrium. The most relevant of these techniques for droplets are:

- **Optical visualization** with optical-wavelength resolution and beyond. These techniques include standard, fluorescence and confocal microscopy^{82,196,197}. The latter allows for 3D visualizations, but the choice of proper dyes is essential, as adding dyes and/or fluorescent molecules (which are often surface-active substances) may cause contamination to the system and artefacts.
- **Digital holographic microscopy** can be seen as complementary to confocal microscopy, focusing on interfaces rather than on the bulk as in standard confocal microscopy. The technique — developed to maturity in the early 2000s and up to now mainly used in the biological context^{198–200} — is crucial and ideal for high-precision measurements and visualizations of growing and shrinking droplets with small contact angle, having a subnanometre in-depth resolution.
- **Microparticle image velocimetry**²⁰¹ makes it possible to obtain information on the velocity fields in and around droplets, even if they are moving, growing or shrinking.
- **High-speed imaging** with frame rates up to several million frames per second²⁰² and **stroboscopic illumination** by nanosecond laser pulses^{203,204} allow for excellent temporal resolution. These techniques also include fluorescent high-speed imaging²⁰².
- **Atomic force microscopy (AFM)** allows for nanometre or even atomic resolution both laterally and in depth. Since the early 2000s, it has developed such that it can now routinely also be used in the liquid phase¹¹. With techniques such as shock-freezing²⁰⁵ or instantaneous polymerization with the help of ultraviolet (UV) radiation¹¹, the nucleation and growth process of droplets can be terminated. The latter requires the use of UV polymerizable liquids as solutes. After solidification of the sessile droplet phase using UV radiation, the other liquid phase can be removed, paving the way for AFM of a solid phase in air, which is much easier than AFM of a liquid phase in another liquid.
- **Surface-enhanced Raman spectroscopy (SERS)**²⁰⁶ allows the chemical composition of sessile droplets or bubbles to be followed in time.
- **Microfluidics** involves well-defined channels and substrates with designed structures and chemical patterns, made possible by microfabrication techniques^{207–212}, in which to study the growth and collective interactions of bubbles and droplets.

Marangoni velocity V_M at the equator of the droplet or, in dimensionless form, the (Marangoni–)Peclet number $Pe_M = V_M R/D$. Here D is the diffusivity. If large enough, that is, for a large enough concentration gradient, this Marangoni flow can make the droplet jump upwards in the stratified density gradient, against gravity¹⁶.

In more detail, what happens is the following series of events that we describe for the concrete example of an anise oil droplet in a stratified (fully miscible) mixture of water (bottom) and ethanol (top) with constant density gradient in between¹⁶ (FIG. 1a–c). First, the oil droplet sinks in the gradient region, trying to find its equilibrium position with respect to density. Ethanol-rich liquid is entrained downwards during this motion. This entrainment is enhanced by the Marangoni flow along the drop surface, from the ethanol-rich top (low surface tension) to the ethanol-poor bottom, leading to further entrainment of ethanol-rich liquid. As the droplet asymptotically approaches the density-matched position, the self-enhancing Marangoni flow eventually overcomes the sinking-induced buoyancy jet. This positive feedback leads to a linear instability and exponential growth of the Marangoni flow, which pushes the liquid

around the drop downwards and thus the drop upwards, like a microswimmer in the pulling mode³. Once this Marangoni flow is dominant (typically after ~60 s), the drop shoots upwards towards the low density region and the process can start over. Up to 6 h of consecutive jumps have been observed. The process only comes to an end once the jumping droplet has sufficiently mixed the stratified liquid. The system can be seen as a canonical example of the competition between Marangoni (surface tension forces) and Rayleigh (gravity). We discuss further examples in other subsections.

In general, the velocity U of a droplet in a concentration gradient ∇c is described in terms of its mobility M , namely $U = M \nabla c$, with the mobility being determined by the droplet radius R , the dependence of the surface tension σ on the concentration c , and the dynamic viscosities $\eta_{i,o}$ of the inner and outer liquid, $M = R\partial_c\sigma/(2\eta_o + 3\eta_i)$ (REFS^{15,17–19}), provided no other phoretic forces play a role.

Flow driven by concentration gradients and restricted to a few nanometre close to a solid interface is called diffusiophoresis^{17,18,20,21}. This term in particular refers to the motion of a colloidal particle in a concentration gradient. Although both

Marangoni flow and diffusiophoresis originate from the interplay of surfaces with compositional gradients, we do not focus on diffusiophoresis in this Perspective, as in general the term refers to liquid–solid interfaces and not to droplets. Note, however, that there are some exceptions; for example, in REFS^{22,23} the movement of a charged oil droplet in a solute gradient is referred to as diffusiophoresis, because in that case a discontinuity in the flow velocity across the droplet interface arises, while the hydrodynamic stresses at the interface are continuous (see FIG. 1 of REF.²³).

Coalescence of droplets of different liquids.

A concentration gradient can instantaneously be imposed by a collision of two droplets consisting of two different liquids. In the

case of coalescence of fully miscible droplets, the surface tension difference at the interface leads to Marangoni flow, with the droplet with smaller surface tension being pulled over the droplet with larger surface tension. In general, the force that counteracts this motion is viscous in nature. The droplets can be sessile^{24–26} or pendent²⁷ from a nozzle with a large contact angle, or even hitting each other in flight^{28,29}, or — with both droplets sessile — sitting on top of each other³⁰ (FIG. 2).

Note that the droplets need not be of equal volume. For example, a droplet can coalesce with a pool of a different liquid (FIG. 2b). In that case, for large enough Ohnesorge and Marangoni numbers (in other words, dominance of Marangoni forces), the spreading front $L(t)$ displays

a universal scaling law $L(t) \sim t^{3/4}(\Delta\sigma)^{1/2}/(\rho\eta)^{1/4}$ or $L(t)/R \sim (\text{Ma}/\text{Sc})^{1/2}(t\nu/R^2)^{3/4}$ over many orders of magnitude^{27,31,32}. Here, ν is the kinematic viscosity and Sc is the Schmidt number (see BOX 1). For sessile droplets (FIG. 2a), the dynamics can be much richer, as, depending on the surface tension difference $\Delta\sigma$, it can show either enhanced coalescence similar to the case of a droplet coalescing with a pool of a different liquid (FIG. 2b), or, more remarkably, delayed coalescence, owing to a competition between capillary pressure and dynamic pressure, induced by the Marangoni flow (FIG. 2a).

The situation becomes further complicated once the different liquids in the drops react with each other³³ or a solidification is induced (for instance, with crosslinkers)²⁹ (FIG. 2c). Then the crucial parameter is the Damköhler number, which compares the timescale of the chemical reaction with that of the hydrodynamics. Yet another situation occurs when a larger sessile droplet is immersing a smaller one of a different liquid (FIG. 2d). When the two three-phase contact lines touch each other, for certain combinations of surface tensions part of the interior sessile droplet can be ‘spat out’ by the larger one³⁰ (FIG. 2d).

Droplets in concentration gradients

emerging from chemical reactions. In the examples of the two previous subsections, the concentration gradient leading to Marangoni flow was imposed from outside. However, such a gradient can also evolve, owing to chemical reactions, for example. A famous example for such gradients can be achieved with so-called Janus particles — that is, particles with different chemical composition on different sides³⁴. In one example, one side of the Janus particle consisted of gold and the other of platinum³⁴. When put in a H_2O_2 solution, catalytically generated oxygen nanobubbles emerged on the Pt side, leading to a chemical potential gradient, which induced a (generalized) Marangoni flow along the particle surface, pushing the particle backwards. There are many variations of such systems, employing the concentration gradient between front and rear, for example in REFS^{35–38}. Note that only very small gradients $\nabla\sigma$ in surface tension are required to drive visible motion of the microparticles⁴.

For Janus particles, the symmetry breaking is imposed on the particle. However, even more interestingly, such symmetry breaking leading to a gradient in concentration around a particle or droplet can also emerge spontaneously,

Box 3 | Numerical tools to address physicochemical hydrodynamics

Alongside progress in experimental techniques (BOX 2), progress on the numerical side has also been crucial in pushing the field ahead. Next to the ever-increasing raw computational power, the development of new numerical methods and open-source codes and tools also contributed to this progress. These now often make possible a one-to-one comparison between experiment and numerical simulations.

The main challenge for the numerical simulations in physicochemical hydrodynamics is the vastly different timescales for the momentum transfer and for the mass transfer, reflected in the large Schmidt number $\text{Sc} \approx 10^3$. This difference in timescales implies that the concentration field must live on a smaller grid than the velocity field, and that the stepping timescale is extremely small. In this scenario, multigrid resolution techniques are a possible way out²¹³. These can be used for various numerical schemes.

The most relevant techniques for the numerical simulations in physicochemical hydrodynamics are:

- **Finite element methods:** moving droplets or droplets with mass-exchange require a well-resolved interface with the surrounding phases. This can be achieved with a sharp-interface finite element method, in which the mesh always conforms to the interface²¹⁴. Because in general the droplet moves, this method requires co-moving all mesh nodes accordingly with the interface. To that end, with Eulerian–Lagrangian methods originally developed for fluid–structure interaction^{215,216}, the mesh can be treated as a pseudo-elastic body, so that the bulk nodes follow the motion of the interfacial nodes, which is connected via Lagrange multipliers to the kinematic boundary condition of the interface²¹⁴. This technique has proved extremely versatile for binary and ternary droplets^{16,82,86,91}, but the challenge remains to efficiently parallelize such codes.
- **Finite difference (FD) with immersed boundary methods (IBM)**^{213,217} are an alternative to finite element methods, allowing for massive parallelization and the calculation of tens of dissolving or growing droplets over a long time^{73,75}. Just as in finite element methods, a weak point of such simulations is that they require a priori input in what mode (for example, constant contact angle (CA-mode) versus constant contact radius (CR-mode)^{8,11}) droplets or bubbles grow or shrink.
- **Phase field methods and Cahn–Hilliard-type approaches**²¹⁸ use a diffuse interface, but readily allow description of spontaneous phase separation and nucleation, such as those occurring in the ouzo effect¹³⁹.
- **Level-set methods**^{219,220} have the advantage that the interfaces between the different phases are sharp. They have been extended to include phase changes and interfacial flows driven by surface tension gradients^{221,222}.
- **Lattice Boltzmann methods**²²³ — coarse-grained versions of the molecular theory of fluids, enabling massive parallelization — have been adopted and applied to multiphase flows^{224,225}, including the selective evaporation or dissolution of multicomponent droplets²²⁶.
- **Molecular dynamics (MD) simulations**^{227–230} have the advantage that they do not require predetermination of whether the (sessile) droplet grows or shrinks in the CA or CR mode as in FD+IBM; instead, the mode emerges from the respective chemical properties of the substrate and the liquids involved^{231,232}. The downsides of MD are that only small nanodroplets (~50 nm) can be simulated, one is restricted to short physical times of, at most, microseconds, and molecular interaction potentials are needed, which are not from first principles.

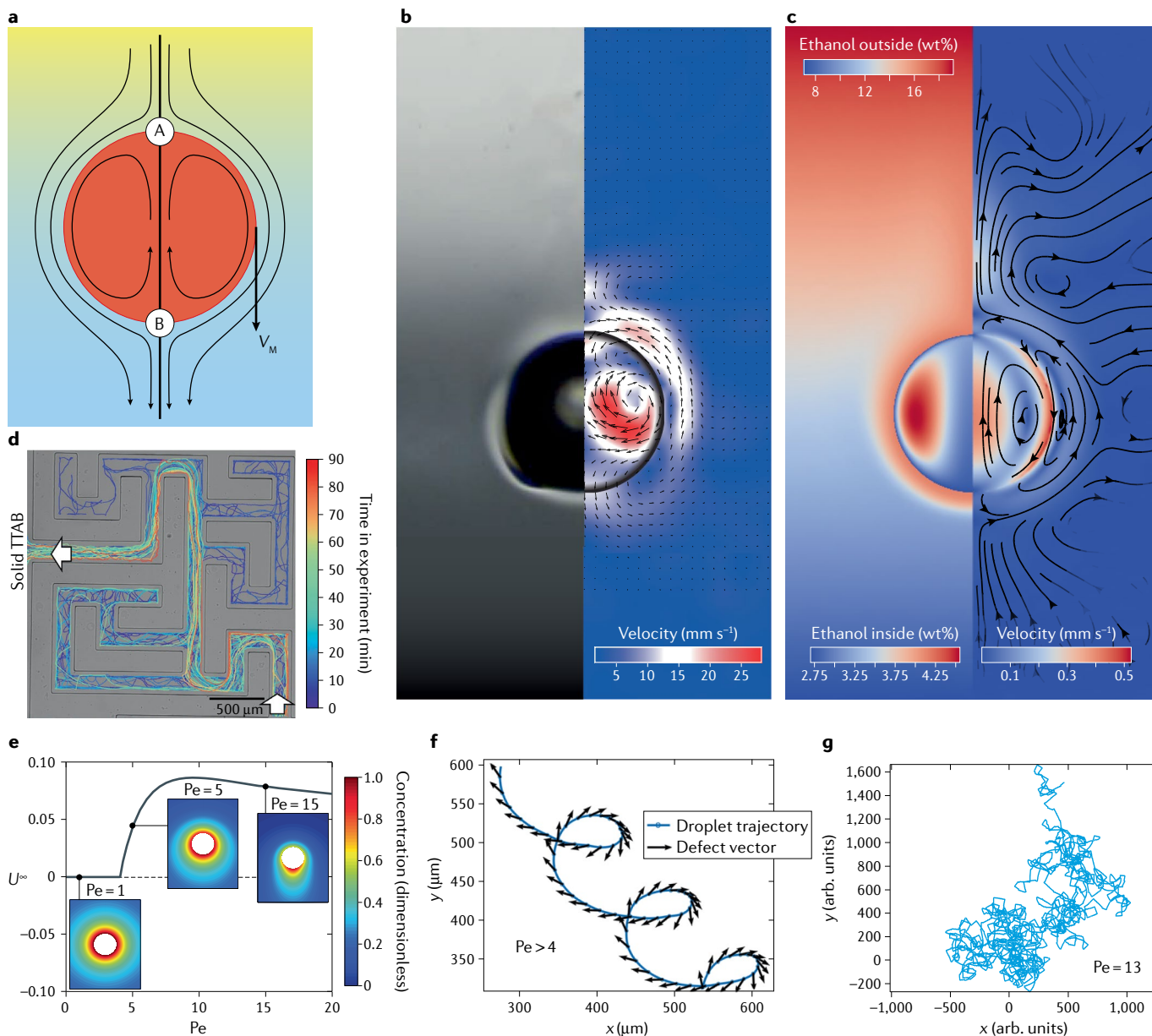


Fig. 1 | Immiscible droplets in the bulk, driven by physicochemical hydrodynamical effects. **a** | Immiscible droplet (red) in a concentration gradient, with the heavier water at the bottom (blue) and the lighter ethanol at the top (yellow). The surface tension at the top of the drop (point A) is smaller than at the bottom (point B), leading to some Marangoni flow, indicated by streamlines in the frame of reference of the drop (calculated in the viscous limit, assuming constant density¹⁵). Also shown is the Marangoni velocity V_M . **b,c** | Velocity fields for a more complicated configuration of a partially (but poorly) miscible anise oil drop in an ethanol–water concentration gradient are shown in panel **b** (experimental, from a snapshot and from particle image velocimetry images) and panel **c** (numerical result). On the right of each of these images, the velocity field is shown, both as colour code and as streamlines (in the lab frame). On the left, in panel **b** the snapshot is shown and in panel **c** the ethanol concentration inside and outside the anise oil drop (also

shown in the lab frame). This situation is described further in REF.¹⁶. **d** | Maze solving by chemotactic droplet swimmers. A chemical gradient of the ionic surfactant tetradecyltrimethylammonium bromide (TTAB) was imposed; the oil droplet propelling in the gradient inside the maze consists of the nematic liquid crystal 4-pentyl-4'-cyano-biphenyl. The trajectories of the swimmers that passed both entrance and exit points are shown. **e** | Spontaneous swimming velocity in the long time limit (U^∞) as a function of the Peclet number Pe . A bifurcation towards droplet motion owing to spontaneous symmetry breaking is seen at $Pe = 4$. **f** | Curling nematic droplet (radius $R \approx 25 \mu\text{m}$, phoretic), in which the Peclet number is estimated to be larger than 4. **g** | Chaotic droplet motion for a phoretic droplet with an even larger Peclet number, $Pe = 13$. Panel **d** reprinted with permission from REF.⁶¹, PNAS. Panel **e** adapted with permission from REF.³⁹, AIP Publishing. Panel **f** reprinted with permission from REF.⁴⁸, APS. Panel **g** reprinted with permission from REF.⁵⁰, APS.

owing to an instability. It has been shown theoretically³⁹ that for large enough Peclet numbers the combined effect of solute dissolution (solubilization) or solute reaction at the droplet interface and Marangoni

flow can produce an instability, resulting in spontaneous and self-sustained motion of the initially isotropic droplet^{19,40–43}. Here the Peclet number is defined by the mobility M of the droplet, the surface

emission rate α (REF.³⁵) and the droplet radius R , namely $Pe = \alpha MR^2/D^2$. The crucial mechanism is that nonlinear mixing of the dissolved substance or the reagent establishes the gradients in concentration, which then are

converted into flow by Marangoni forces or diffusiophoresis^{17,44–47}. The bifurcation diagram of this process and the resulting swimming velocities are shown in FIG. 1e, along with the concentration fields around the droplets for various Peclet numbers. They and FIG. 1a also give an idea of the flow field around the swimming droplet. For even larger Peclet numbers, the droplet can curl⁴⁸, swim helically⁴⁹ or even chaotically^{49,23,50}; (FIG. 1f,g). Once two or more such droplets are close to each other, they show rich and non-trivial collective behaviour^{51–54}.

The solubilization or chemical reactions at the droplet interface can be of various natures. Many examples are given in the review article of REF.⁴. These examples include simply dissolving or slowly reacting droplets, but also micellar

solubilization^{55,56} of a surfactant on the oil droplet well above the critical micelle concentration, nematic liquid crystal droplets self-propelling in a highly concentrated surfactant solution^{48,49,57}, droplets with a surfactant undergoing a chemical reaction⁵¹, binary droplets with selective dissolution⁵⁸ and many others⁴. The driving strength of solubilization or dissolution decreases as function of time, and the droplet shrinks, leading to transitions in the motion pattern, for instance from random, to helical, to straight⁴⁹, but this process is slow and can take many hours. An interesting case is when the droplet crosses its own trace. Another startling case is a surface-active chemotactic droplet that is able to navigate through a complex maze, thanks to an

imposed concentration gradient and the self-propelling property^{59–61} (FIG. 1d).

Droplets in concentration gradients emerging from phase transitions. The simplest case of a droplet in an out-of-equilibrium situation may be a volatile droplet evaporating in air or a soluble droplet dissolving in another, originally pure liquid. For a spherical droplet in the bulk of a host liquid, this problem has been analytically solved⁶². That calculation was originally made for dissolving bubbles but later generalized to dissolving droplets⁶³. The evaporation or dissolution of a single sessile droplet consisting of a pure liquid in a solvent has meanwhile been reasonably well understood^{8,9,11,64–69} — even if it is not purely diffusive, and thus convective effects

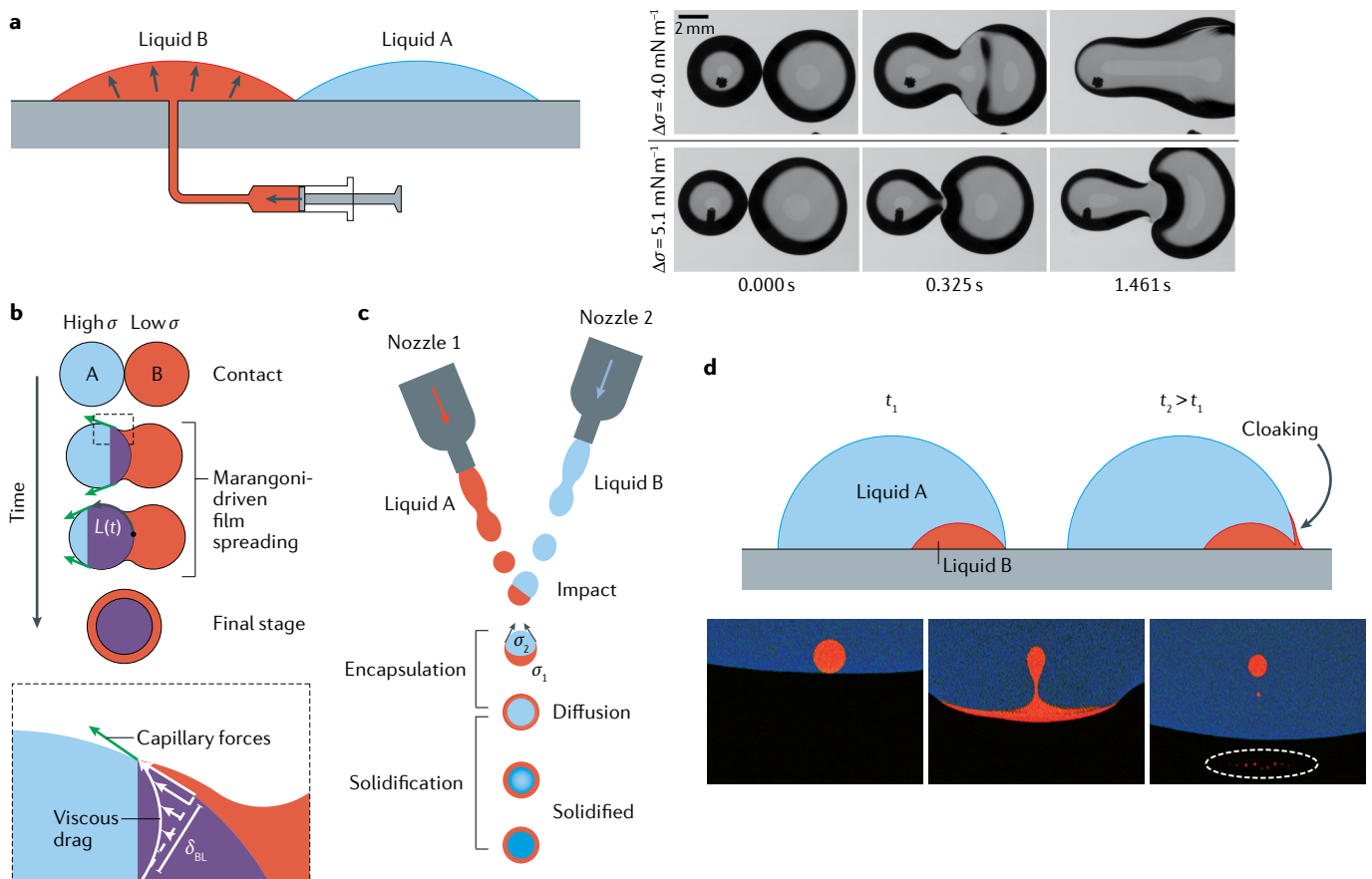


Fig. 2 | Various types of coalescence of two droplets consisting of different liquids. **a** | Side-view sketch of a coalescent experiment of two sessile droplets^{25,26} (left panel). Droplet A is first deposited from above, then droplet B is created and grown by pumping fluid from below the substrate. The outcome is shown in the right panel, where we show top-view snapshots for two different surface tension differences $\Delta\sigma$, which are established with different 1,2-butanediol/water mixtures, featuring enhanced (upper row) or delayed (bottom row) coalescence. **b** | Side view of two pendent droplets²⁷, with the one with lower surface tension σ creeping over the one with higher surface tension, described by the spreading front $L(t)$. A detailed sketch of the process is shown in the lower panel, with the viscous velocity profile over the boundary layer of thickness δ_{BL} caused by the viscous force, counteracting the

Marangoni force. In this case, the Marangoni force wins, leading to encapsulation. **c** | Likewise, an encapsulation is also possible for jetted droplets of different liquids²⁹. In this case, one droplet contains a cross-linker and the other a polymer, such that their coalescence leads to solidification. **d** | Snapshots (at two different times t_1 and $t_2 > t_1$) of another geometry of droplet–droplet interaction, namely one sessile droplet sitting on another smaller one. When the two three-phase contact lines touch each other (left, t_1), part of the smaller droplet can be ‘spat out’ (right, t_2). Three confocal images at consecutive times are shown in the lower panel. The dashed oval marks spat-out microdroplets. Panel **a** (left) adapted with permission from REF.²⁵, ACS. Panel **a** (right) adapted with permission from REF.²⁶. Panel **b** adapted with permission from REF.²⁷, RSC. Panel **d** adapted with permission from REF.³⁰, RSC.

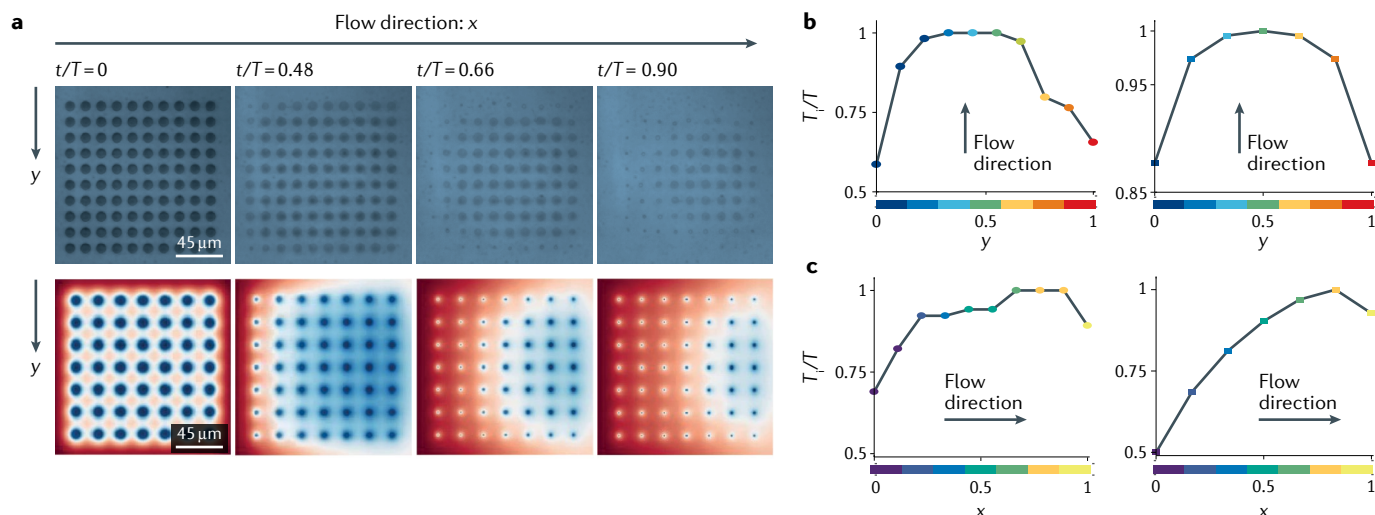


Fig. 3 | Collective dissolution for droplets. a | Time evolution of droplet dissolution. The upper row shows consecutive snapshots for a 10×10 array of oil droplets, with a spacing of $5 \mu\text{m}$, for a flow rate of $200 \mu\text{l min}^{-1}$ (corresponding to a Peclet number of $\text{Pe} = 237$) for four different times t , normalized using T , which is the total time for the droplet array to completely dissolve. The lower row shows a pseudocolour plot of the concentration field from numerical simulations for a 7×7 droplet array for flow conditions

corresponding to those in experiments. Blue corresponds to oil and red corresponds to water. The water is injected into the chamber along the x direction. **b, c** | Total dissolution time (T) of droplets along the span-wise direction y (panel **b**) and the stream-wise direction x (panel **c**). In panels **b** and **c**, on the left the experimental data are shown, and on the right the numerical. Figure adapted with permission from REF.⁷⁵, RSC.

outside the droplet due to density differences of the liquids come into play⁷⁰, enhancing the dissolution.

The situation becomes more interesting once multiple dissolving or evaporating sessile droplets interact, as in general they shield each other. The reason is that dissolving neighbouring droplets reduce the concentration gradient at the interface and thus the outflux from the droplet, leading to longer (and heterogeneous — depending on the position of the droplet) lifetimes^{71–77}, even when the solvent is flowing over the sessile droplets⁷⁵. Such a situation has recently been explored both experimentally and numerically, with reasonable agreement (FIG. 3). Note that the dissolution delay by shielding only holds in the pure diffusive regime. Once convective effects (that is, density differences within the surrounding liquid with large resulting Rayleigh numbers) come into play, remarkably, collective effects can also enhance dissolution, owing to the collective interaction of individual density plumes⁷⁷.

Coming back to single sessile droplets, concentration gradients can also emerge from selective evaporation (or dissolution) from a sessile binary droplet, or — again more generally — a droplet consisting of several miscible liquids. The reason for this phenomenon lies in a combination of the (in general) different volatility of the components and the singularity of the evaporation (or dissolution) rate at the rim of the droplet^{8,65,67,78} (provided the contact

angle is smaller than 90°), leading to a concentration gradient at the interface of the droplet. The resulting surface tension gradient drives a Marangoni flow inside the droplet^{79–92} (FIG. 4a). This effect is similar to what leads to the ‘tears of wine’⁹³ inside a partially filled wine glass. In that case, selective evaporation of ethanol at the edge of the meniscus leads to locally larger surface tension, which thus pulls part of the remaining wine upwards along the alcohol-wetted glass, finally leading to an instability of the film and droplets sinking down the glass wall. In evaporating droplets, the Marangoni convection can be so violent — with velocity exceeding millimetres per second — that the axisymmetry breaks^{83,86}. The same can happen through moisture absorption: the absorption of water vapour (that is, moisture) to a sessile or pendent glycerol droplet can lead to an axisymmetry-breaking Bénard–Marangoni instability of the resulting flow, which is driven by water concentration gradients at the droplet–air interface, emerging from preferential absorption of the water at the rim of the droplet⁹⁴. The evaporation, absorption and dissolution dynamics of multicomponent sessile droplets is an active area of research.

Depending on the nature of the two components of the binary liquid, the (stronger) evaporation of one component can lead to several different scenarios for the physicochemical hydrodynamics of the sessile binary droplet. In one scenario^{88,89,95},

the selective evaporation of one liquid can lead to segregation of this liquid in the centre of the droplet thanks to shielding by the other, non-volatile liquid. This scenario occurs once the Marangoni flow arising through concentration differences at the droplet–air interface is too weak to fully mix the two liquids.

An even more interesting second scenario comes into play once the two miscible liquids of the binary droplet display a sufficiently large density gradient^{90,91}, as can become the case for a droplet consisting of water and glycerol⁹¹, for example. This density gradient is ‘activated’ by selective evaporation of the more volatile liquid, which in REF.⁹¹ is water. In dimensionless form, the density gradient is expressed as Rayleigh number Ra . The gravitational forces resulting from the density gradient compete with the Marangoni forces on the droplet–air interface, the strength of which in dimensionless form is expressed as the Marangoni number Ma . Once the gravitational forces win, Rayleigh convection rolls dominate, and the flow pattern in sessile droplets (FIG. 4b) is both qualitatively and quantitatively different from that in pendent droplets (FIG. 4c). For submillimetre droplets, this difference is remarkable because the Bond number of such droplets is $\text{Bo} \ll 1$, on first sight implying that gravity does not play a role — but only as compared with capillarity (implying the spherical cap shape of the droplet), not as compared with viscosity. The full phase

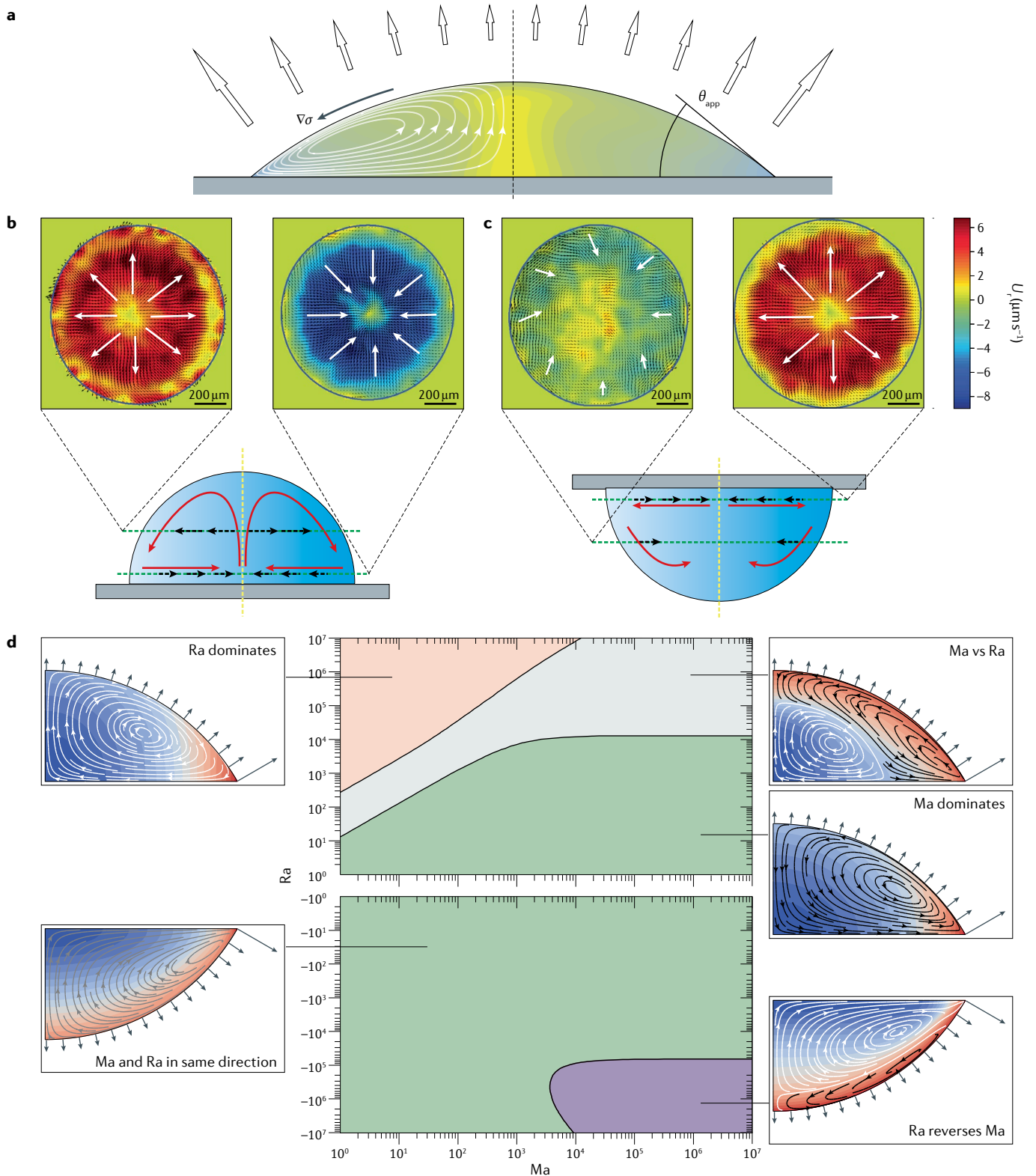


Fig. 4 | Multicomponent droplet evaporation. **a** | Evaporation of a 5- μl binary droplet consisting of ethanol (0.1%) and water. The higher evaporation rate at the rim and the selective evaporation of the ethanol leads to a surface tension gradient $\nabla\sigma$ at the droplet–air interface, driving Marangoni convection inside the droplet, indicated by white flow lines. Note that for larger driving (that is, larger Marangoni number), the axisymmetry of the process breaks. θ_{app} , contact angle. **b,c** | The evaporation of a binary sessile droplet (panel **b**) and of a binary pendent droplet (panel **c**). Upper images

are top-down views at heights indicated by the green lines in the schematics (lower images). The different flow patterns for sessile and pendent droplets reveal that gravity (pointing downwards) plays a major role. U_r , radial velocity component. **d** | Phase diagram in the parameter space of Rayleigh number Ra versus Marangoni number Ma , for an evaporating binary droplet. Depending on Ra and Ma , either Rayleigh convection rolls are seen, or Marangoni convection rolls, or both²³³. We also show the respective flow and concentration patterns. Panels **b** and **c** reprinted from REF.⁹¹, APS.

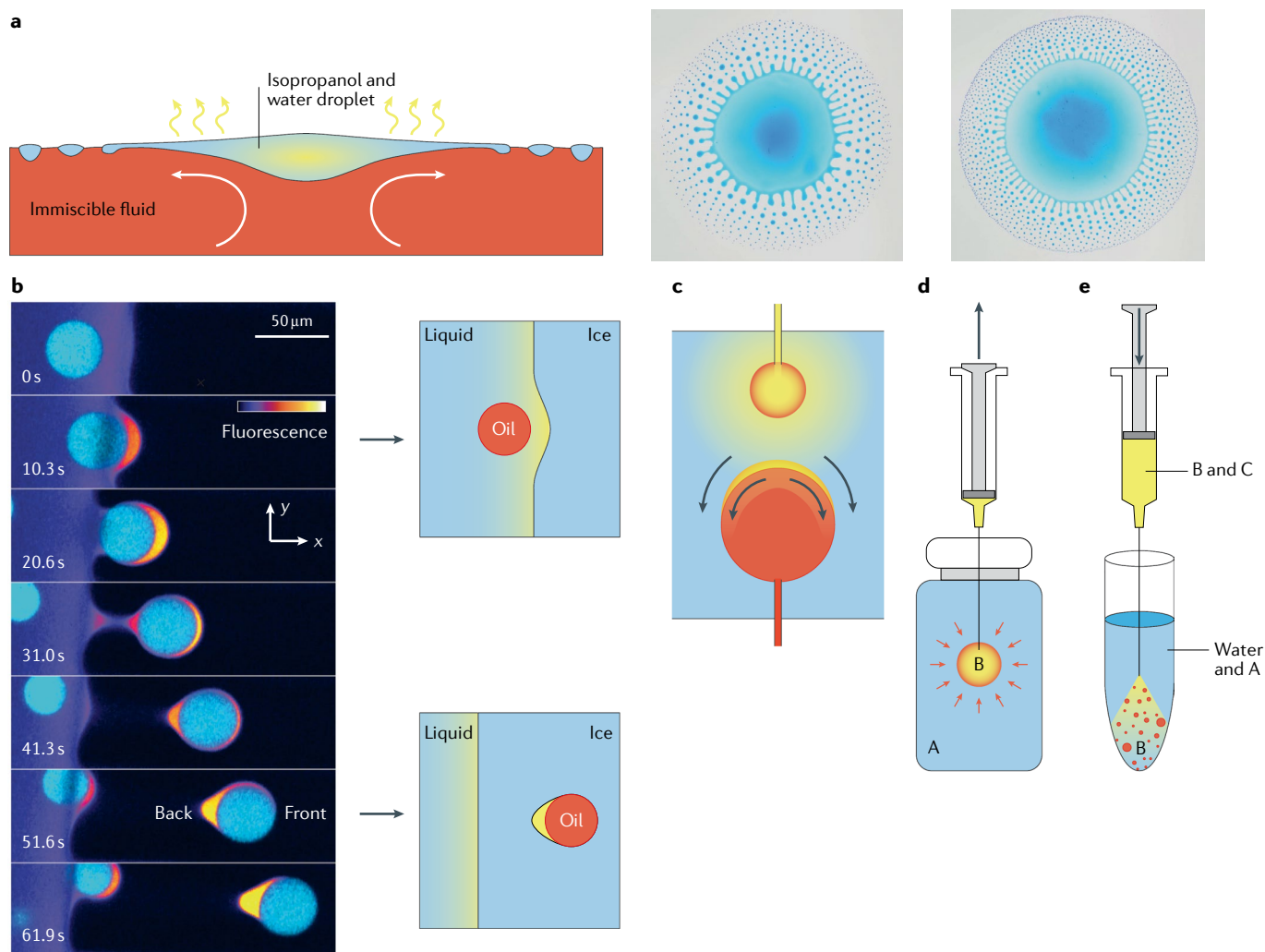


Fig. 5 | Physicochemical hydrodynamical effects evolving phase transitions. **a** | Marangoni bursting: evaporation-induced emulsification of a binary droplet (isopropanol and water) on an immiscible bath. The centre and right panels show top views of the flow pattern for two different isopropanol concentrations of the deposited binary alcohol–water droplet, from lower (centre image, 0.4 mass fraction) to higher (right image, 0.45 mass fraction). **b** | Horizontal cross-section of a typical interaction between a droplet and the solidification front, showing the accumulation of solute and its redistribution around the droplet. In this example, the temperature gradient leading to the freezing is 5 K mm^{-1} , with a sample velocity of $2 \mu\text{m s}^{-1}$. The inset sketches visualize the process at early times (upper inset) and later times when the front has passed over the oil droplet (lower inset). **c** | Two droplets of two different slightly soluble liquids are made to approach each other in a third liquid and interact diffusively, even before they coalesce.

The solubility of the yellow liquid is greater than that of the red one, leading to a concentration gradient of the yellow liquid on the red drop and thus in general to Marangoni forces and the resulting Marangoni flow in the red drop and in between the drops, indicated by the black arrows. **d** | Classical single droplet microextraction¹⁴¹. Solute A (red) dissolved in water (blue) accumulates in a droplet of water-immiscible liquid B (yellow), owing to its higher solubility in B compared with water. After equilibrating, the droplet, consisting of a mixture of A and B, is extracted with a syringe, to be further analysed. **e** | Principle of dispersed liquid–liquid microextraction (DLLME)¹⁴². Substance A is extracted from water (blue) by adding a mixture of liquids B and C (yellow). Owing to the ‘ouzo effect’, droplets of liquid B (red) nucleate and grow. Substance A is more soluble in liquid B than it is in water, so the A–B phase can be extracted by extracting the droplets. Part **a** adapted from REF.⁹⁸, CC BY 4.0. Panel **b** adapted with permission from REF.¹⁰⁴, AAAS.

diagram in the Ra–Ma parameter space features pure Rayleigh convection rolls, pure Marangoni convection rolls or both at the same time (FIG. 4d). Additionally, for large Rayleigh numbers the axisymmetry can be broken, and a Rayleigh–Taylor instability can emerge⁹⁶. Instabilities can also emerge when a binary droplet evaporates on a bath of an immiscible liquid^{32,97,98} (FIG. 5a). Here, similarly to the case of coalescing droplets, the Marangoni stress in the drop pulls the droplet outwards but is balanced

by the viscous stress in the oil bath, leading to a bulk flow (FIG. 5a). The evaporation causes a transition from partial to complete wetting, which sets the radius of the central drop (FIG. 5a). In the limiting case of the bath height approaching zero, the situation is that of a binary droplet on a thin film. In that case, the outwards Marangoni flow can become so violent that a hole emerges in the film⁹⁹.

The dynamics of an evaporating binary sessile droplet, be it on a substrate

or a liquid, is further complicated once surfactants also come into play^{83,87}. In this case, also, the Marangoni driving of the flow can be so strong that its axisymmetry is broken. The surfactants and the composition of the binary droplet also strongly affect the pattern of the deposit, as has been demonstrated with evaporating whisky droplets⁸³.

Note that not only the dissolution of sessile binary droplets with the resulting Marangoni flows is highly non-trivial, as

elaborated above, but even the dissolution of spherical binary droplets in the bulk. The reason is that, owing to selective dissolution, concentration gradients inside the droplet between its surface and its bulk can arise¹⁰⁰. These can lead to considerable memory effects (in particular for small droplets), which do not exist for the dissolution of a pure droplet^{100–102}.

Another example of a concentration gradient (that is, an out-of-equilibrium situation) that emerges from phase transitions is a freezing miscible mixture of liquids with different freezing temperatures. A particularly intriguing case is a pure immiscible droplet in a binary liquid undergoing solidification of one component¹⁰³. In that case, a concentration gradient emerges that acts on the droplet, pushing

it either away from the solidification front or towards it, and possibly finally leading to the engulfment of the droplet¹⁰⁴ (FIG. 5b). A generalization of this problem is freezing colloids, which show extremely rich and intriguing behaviour¹⁰³.

Droplet nucleation and growth in ternary liquids. The examples discussed above dealt with miscible, sparingly miscible and immiscible liquids, but the solubility of one liquid in another was constant in all cases. However, in ternary liquids, this need not be the case. In general, the mutual solubilities depend on the relative concentrations of the liquid. This is commonly expressed in the so-called ternary diagram (FIG. 6a). In particular, the ternary diagram can contain ‘ouzo regions’, in which submicrometre-sized

droplets of one species can metastably exist. The best-known example of such liquids is ouzo itself.

Ouzo is a transparent Greek liquor (equivalently, one can take as examples the French pastis, Italian sambuca or Turkish raki), which chemically — in spite of its actual more complex composition — for the purposes of physicochemical hydrodynamics can be considered a ternary liquid consisting of ethanol, water and (anise) oil. When served, water is usually added, which lowers the solubility of the oil, as described by the ternary diagram (FIG. 6a). Doing so leads to oil oversaturation and subsequently to the nucleation of oil droplets in the bulk liquid and thus to the characteristic milky colour. This process is called the ouzo effect^{105–107}, or solvent exchange or solvent shifting.

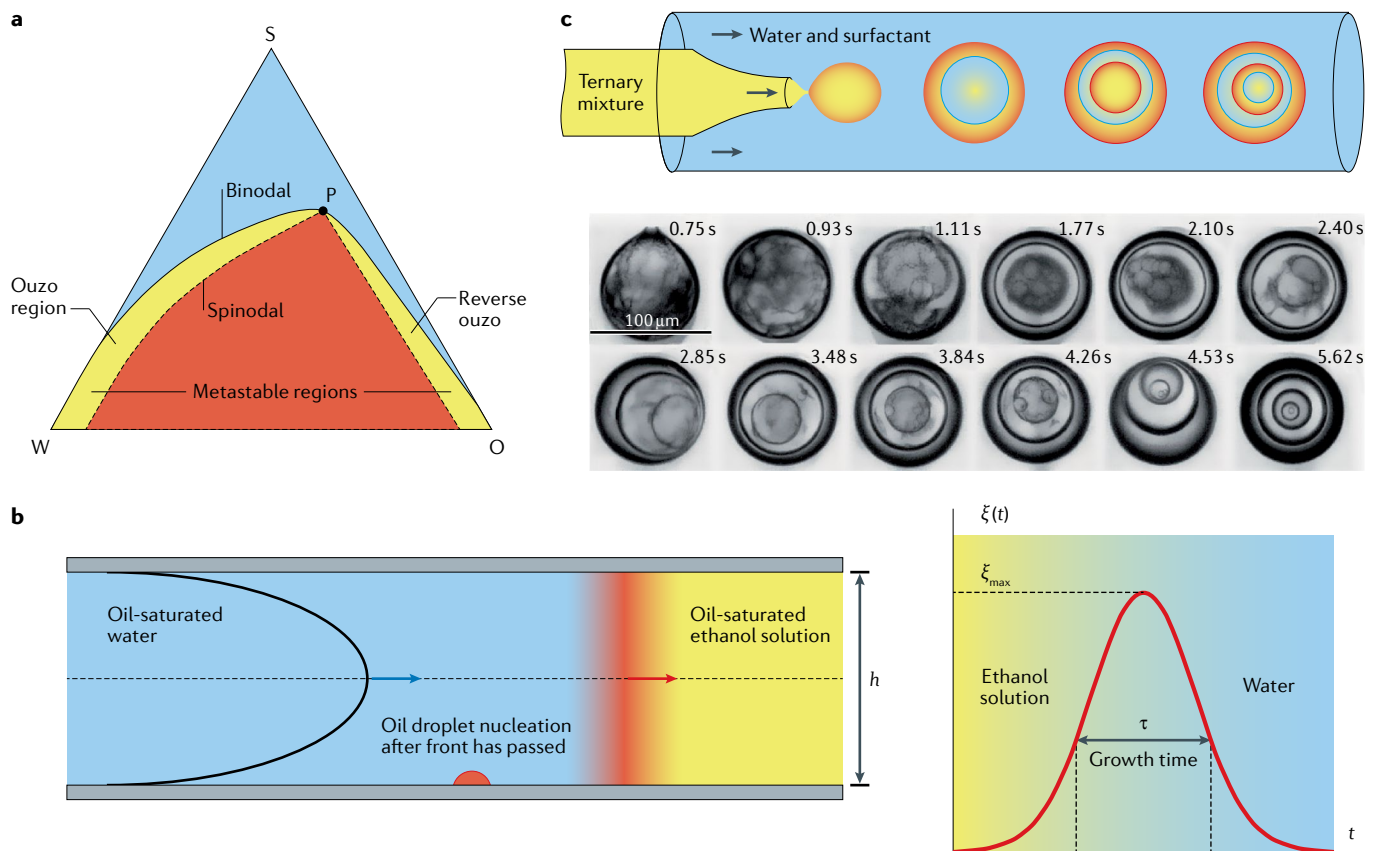


Fig. 6 | Principles of solvent exchange. a | Schematic ternary diagram of a ternary mixture of water (W), a solute (S) such as ethanol and an oil (O) such as anise oil, in the case of ouzo. At the corners, the respective liquid has a 100% concentration. The concentration linearly decreases to zero at the other two corners, along the axes of the triangle. Above the binodal curve, the three liquids are fully miscible (blue region). Below the spinodal curve (red region), water and oil separate into two phases. Between the binodal curve and the spinodal curve, there is a small region (yellow) in which submicrometre-sized oil droplets in water (‘ouzo region’) or water droplets in oil (‘reverse ouzo’) are metastable. More complicated ternary diagrams with ‘pre-ouzo’ regimes with oil nanodroplets in an otherwise miscible regime are possible³⁷. **b** | Principle of solvent exchange. The left panel shows a bad solvent (in this case, water) replacing a good solvent (in this case, ethanol),

leading to a front of oversaturation and thus to the nucleation of (in this case, oil) droplets at the hydrophobic surface. Note that the plug-flow-like nature of the oversaturation front is due to Taylor–Aris dispersion^{118,234–236}. The velocity profile itself remains parabolic. For fixed position at the wall, a front of oversaturation $\xi(t) > 0$ passes by (right panel), leading to droplet growth. **c** | Ternary liquid of oil, water and ethanol brought into contact with an aqueous phase with a co-flow device^{237,238}, leading to phase separation in the emerging droplets, which develop onion-like structures (upper panel). The lower panel shows details of the developing onion-like structures of the phase-separating ternary liquid. The time is given in seconds. The length scale given in the first snapshot at 0.75 s is 100 μm . Panel **a** adapted with permission from REF.²³⁹, Elsevier. Part **b** adapted with permission from REF.¹¹⁶, PNAS. Lower panel of part **c** adapted with permission from REF.¹³⁵, Wiley.

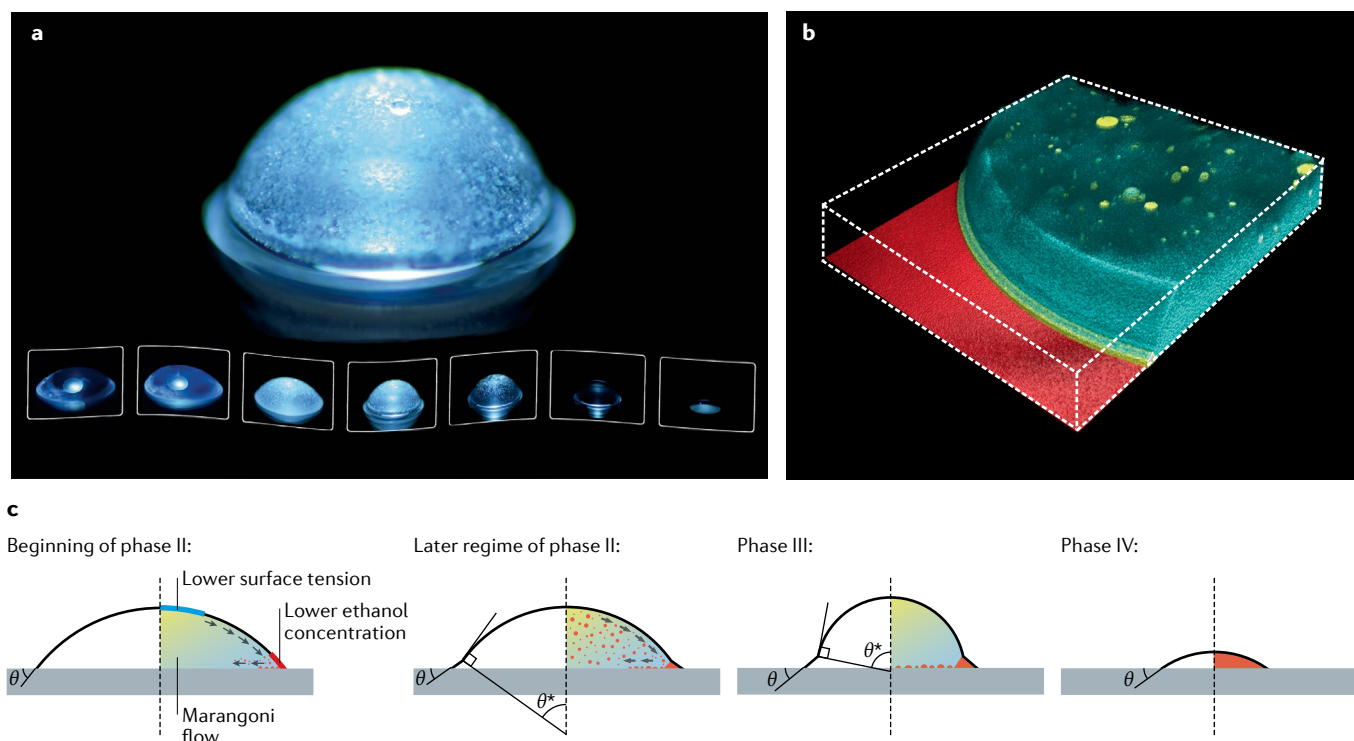


Fig. 7 | **Evaporating ouzo droplet.** **a** | Optical image of phase III of the droplet (phases are defined in panel **c**), with a milky droplet sitting on an oil ring. The insets show earlier and later snapshots of the droplet. **b** | Confocal image early in phase III, when the oil ring starts to develop. **c** | The four sketches show different lifetime phases of the evaporating ouzo droplet. θ and θ^* are the respective contact angles. Yellow indicates ethanol, blue indicates water and red indicates the oil. Figure adapted with permission from REF.⁸², PNAS.

The ouzo emulsion is remarkably stable against Ostwald ripening^{108,109}, that is, the capillary-pressure-driven shrinkage of the smaller droplets and the simultaneous growth of the larger ones. (Such shrinkage and growth is known as coarsening.) Moreover, the nucleated droplets have a relatively sharp size distribution. Both features — the absence of Ostwald ripening and the sharp droplet size distribution — are not fully understood and are active areas of research¹¹⁰.

When the solvent exchange process takes place in the presence of a hydrophobic surface, sessile nanodroplets nucleate at the surface and then grow^{11,111}. This offers the opportunity for a bottom-up approach in ‘building’ droplets or crystals. Nucleation and growth of the droplets strongly depend on the geometrical and chemical nature of the substrate, and pinning of the contact line (or the absence of pinning) plays a paramount role^{112,113} in determining the growth mode of the droplet (constant-contact-radius mode versus constant-contact-angle mode). It is this pinning that enables the stability of surface nanodroplets and nanobubbles against evaporation or dissolution^{11,114,115}.

Advances in modern microfluidics and microscopy of various kinds (see BOX 2)

make it possible to monitor the growth of the nucleated sessile nanodroplets as a function of the control parameters (the most relevant of which are summarized in BOX 1)^{116–119} — including on patterned surfaces^{120,121}, as a function of time¹²², and with collective effects of the nucleating droplets^{123–125}.

The essence of the process is that a bad (but fully saturated with a solute) solvent in a narrow channel of submillimetre height h replaces a good one (also saturated, or at least containing sufficient solute), leading to a front of oversaturation of the solute, which passes by the substrate (FIG. 6b). This passage leads to nucleation of nanodroplets on the substrate (provided the wettability of the droplet liquid on the substrate allows for this) and to their growth. This growth is controlled by the thickness of the diffusive boundary layer around the droplets (which is set by Prandtl–Blasius–Pohlhausen boundary layer theory¹²⁶) and thus the mean flow velocity, or, in dimensionless numbers, the Peclet number Pe . One can theoretically derive $\langle V_f \rangle \sim h^3 Pe^{3/4}$ for the final area-averaged volume $\langle V_f \rangle$ of the droplets, which agrees very well with the experimental data^{118,127}.

The solvent shifting can also be driven by evaporation or dissolution of one of the solvents. Such experiments combine

features of the Marangoni flow in ternary droplets that is triggered by evaporation or dissolution, as described above, with the nucleation of microdroplets triggered by solvent shifting as described here.

An illustrative and simple example for such an experiment is the evaporation of an ouzo droplet on a substrate under ambient conditions^{82,86} (FIG. 7). The evaporation process has four phases. In phase I, the spherical cap-shaped droplet remains transparent, while the more volatile ethanol evaporates. The evaporation occurs preferentially at the rim of the drop, owing to the geometric singularity there, as explained in the previous subsection. This evaporation leads to a local reduction in ethanol concentration and, according to the ternary diagram (FIG. 6a), to nucleation of oil droplets at the rim. This nucleation is the beginning of phase II, in which oil microdroplets quickly nucleate in the whole drop, leading to the typical milky ouzo appearance. These microdroplets can coalesce and form an oil ring at the rim of the droplet (early in phase III). Eventually, all ethanol has evaporated and the drop — which now has a characteristic non-spherical cap shape, with the water drop sitting on top of the oil ring — is thus transparent again (late in phase III). Finally,

in phase IV, all the water has also evaporated, leaving behind a tiny spherical-cap-shaped oil drop. The entire evaporation process takes about 15 minutes. Note that this example of an evaporating ouzo droplet on a substrate can also be numerically treated, by employing finite element methods, resulting in good agreement between numerics and experiments^{82,86}.

There are several variations of the theme of an evaporating or dissolving ternary droplet. In REF.¹²⁸, an ouzo droplet evaporating on a superamphiphobic surface is studied, again both experimentally and numerically. In this case the contact angle is much larger than 90°, resulting in a maximal evaporation rate at the apex of the droplet and accordingly to the start of the oil microdroplet nucleation occurring at that position. The Marangoni flow is also directed towards the apex of the droplet, and not towards the rim, as was the case for contact angles smaller than 90°. In REF.¹²⁹, the dissolution of a water–ethanol drop in a bath of anise oil was analysed. In that case, during the dissolution two types of microdroplet nucleation were observed, namely oil microdroplet nucleation in the aqueous drop (ouzo effect) and water microdroplet nucleation in the surrounding oil (inverse ouzo effect) (FIG. 6a). Again, various physicochemical hydrodynamical processes such as Marangoni flow, Rayleigh convection, diffusion and nucleation compete in an extremely rich way, but can nonetheless be disentangled¹²⁹ by including the key physics in a simple model^{129–132}.

A study of an even richer system with two big drops consisting of different aqueous liquids (one water drop, and one consisting of ethanol–water mixtures) in a bath of toluene as host liquid has been reported¹³³. The diffusion of the aqueous liquids through the toluene leads to the nucleation of aqueous microdroplets (inverse ouzo effect) between the two bigger drops. In a variation of this experiment, two droplets of two different slightly soluble liquids are made to approach to each other in a third liquid (FIG. 5c). Even before the droplets touch (a situation described in the subsection on coalescing droplets), there is diffusive exchange of matter. If one liquid has higher solubility than the other, the result is a concentration gradient of the more soluble liquid on the drop of less soluble liquid, and thus, in general, Marangoni forces and Marangoni flow in the less soluble drop and between the drops (FIG. 5c). This flow greatly changes the diffusive process and the forces between the droplets. In the case of ternary liquids with a solubility gap, an experimental

set-up as sketched in FIG. 5c can also lead to nucleation of microdroplets, as in REF.¹³³.

Droplets of ternary liquids can phase-separate in many different ways^{110,134–139}, showing rich and complex behaviour. For example, a miscible droplet of diethylphthalate (DEP) oil, water and ethanol, which has a ternary diagram similar to that shown in FIG. 6a, demixes on contact with an aqueous phase, to give alternating, onion-like layers of oil and water^{135,139} (FIG. 6c). The detailed dynamics of this liquid–liquid phase separation and the type of emerging structures strongly depends on the exact relative initial composition of the ternary liquid and the viscosities of all involved liquids. The process is controlled by the diffusion of water into the ternary droplet and, vice versa, of its components out of the droplet. The liquid–liquid phase separation can be modelled with Cahn–Hilliard-type approaches¹³⁹.

A microfluidics co-flow device similar to that of FIG. 6c, operated with ternary liquids, is also well suited to impose a well-defined concentration gradient, in order to quantitatively study the competition between diffusion, Marangoni convection and nucleation of microdroplets in the ouzo region or inverse ouzo regime of the ternary diagram¹⁴⁰. With the controlled and laminar flow profiles of such a device, detailed experimental information on the conditions for droplet formation and their radial migration in the ternary flow can be obtained and compared with the ternary phase diagrams.

Relevance and applications

Having shown some examples of recent fundamental work on physicochemical hydrodynamics in well-defined droplet systems in the previous section, we now come to the relevance of multicomponent droplet systems in applications. In the Introduction, we already mentioned various application fields. In the following, we go into more detail for five quite different application fields. We cannot be encyclopaedic, nor go into depth, but we hope to convey the flavour of the applications and their great potential. Because in the previous section we ended with ternary droplets with a solubility gap, here we continue with them, and only then come to miscible binary and multicomponent droplets.

Chemical analysis and diagnostics. Liquid–liquid extraction — the transfer of a solute from one solvent to another — is one of the core processes in chemical technology

and analysis. For chemical analysis such as chromatography, ever since the pioneering work of the Nobel laureate Fritz Pregl¹⁴¹ on microanalysis, there have been continuous efforts to further miniaturize the extraction process of the analyte and to optimize the extraction recovery and preconcentration factor. Demands for miniaturization have continued to increase¹², reflecting the urgency of the problem. First, the need to detect trace quantities of some substance is still increasing in medical, biomedical, food safety and environmental contexts. Additionally, the health monitoring systems of the future will be based on rapid measurements on small sample volumes. Finally, miniaturization will lead to reduced chemical waste and environmental strain, in other words, towards ‘greener’ analytical methods and process technologies.

Since the early 2000s, ‘single-drop microextraction’¹² has become popular for sample preparation of trace organic and inorganic analysis. The principle of this method (FIG. 5d) is that a solute A dissolved in water accumulates in a droplet of water-immiscible liquid B, owing to its higher solubility in B as compared with water. After an equilibrium has been achieved, the droplet, which now consists of a mixture of A and B, is extracted with a syringe, to be further analysed by methods such as chromatography. The scale on which single-drop microextraction can be done remains limited, but this limitation is overcome in the modern technique of dispersive liquid–liquid microextraction, which was first reported in 2006 (REFS^{142–144}) and makes heavy use of the solubility gap of ternary liquids and thus the ouzo effect, discussed above. In this method, a mixture of two miscible liquids B and C (with low concentration of B) is put into water containing the analyte A, with B being immiscible with water (say, carbon tetrachloride¹⁴⁴), but liquid C being miscible (say, acetone¹⁴⁴) (FIG. 5e). When poured into the aqueous solution containing A, droplets of liquid B immediately nucleate and then further grow out of the oversaturated solution. The liquid B is chosen such that it has much higher solubility for the analyte A than water does and is heavier than water and liquid C. The large total surface area of the nucleated microdroplet ensemble greatly helps the extraction process. The final step is to centrifuge the dispersion and take out the A–B phase.

The relevant parameters to characterize the performance of liquid–liquid extraction processes are the preconcentration factor,

defined as the ratio of the analyte concentration in the centrifuged droplets, and the extraction recovery, defined as the percentage of analyte that could be extracted. Hitherto, it has not been possible to calculate these parameters a priori, hindering the optimization of liquid–liquid extraction processes, which is often done by trial and error. Liquid-handling robot systems¹⁴⁵ have even been built to automate the evolutionary process of finding the optimum. Clearly, a quantitative understanding of the nucleation and the diffusive dynamics of droplets in ternary systems is crucial to make progress towards a quantitative understanding and systematic optimization of dispersive liquid–liquid microextraction.

Another diagnostic application of the physicochemical hydrodynamics of droplets far from equilibrium is nanoextraction of tracers¹⁴⁶. Sample preparation is considered to be the most difficult step in an analytic workflow. Current methods for extraction and separation of minute amounts of substances in liquid samples are laborious, time-consuming, often involve large amounts of toxic organic solvents and are difficult to automate, implying high labour costs. However, liquid–liquid extraction and online analysis of traces of analytes in aqueous solutions, including in biomedical, health, pharmaceutical and environmental contexts, may be greatly improved by surface-nanodroplet-based sensing techniques^{147–149}. Surface nanodroplets pre-formed by solvent exchange on a substrate within a microflow channel are the basis for such nanoextraction. The principle is that the partition coefficient of the compound in the droplets is much higher than in the solution. The compound in the liquid can thus be extracted into the surface nanodroplets and be quantified by surface-sensitive spectroscopic techniques¹⁴⁹. This approach can potentially achieve extraction-detection of analytes at extremely low concentrations in one single and simple step, allowing for fully automated sample analysis through programmable nanodroplet production for extraction and in situ detection.

Pharmaceutics, and chemical and environmental engineering. The ouzo effect is relevant not only for microextraction in chemical analysis and diagnosis, but also for drug production and delivery¹⁰⁷ and in pharmaceutical science and cosmetics¹⁵⁰, providing a basis for the preparation of pharmaceutical products, formulation of cosmetics and insecticides, liquid–liquid extraction and many other practical processes. In this context, the ouzo effect

is also called ‘nanoprecipitation’. Small hydrophobic organic molecules, lipids or polymers exhibit similar microphase separation and, when mixed with a poor solvent, form nanodroplets or nanoparticles with homogeneous sizes. Note that often the details of the mixing process matter. Why this is the case has not yet been fully understood. For example, in some cases the mixing must be very rapid — a process called ‘flash nanoprecipitation’, which has been demonstrated to be a simple way to produce drug-loaded polymeric nanoparticles, protein nanoparticles and other multifunctional colloids with narrow size distribution^{151–153}. Droplet formation by solvent exchange is also highly relevant for separation and purification in other applications of the chemical and pharmaceutical industry, including the undesirable phenomenon of oiling-out crystallization in production of pharmaceutical ingredients, amino acids and proteins¹⁵⁴.

On a larger scale, understanding and controlling nucleating and growing droplets in liquid–liquid phase separation is essential for improving the efficiency of industrial operations, for example in the extraction of natural resources, recycling of valuables from waste and removing organics in waste water treatment, in flotation and in renewable energy technologies. Finally, dilution-induced phase separation (that is, the ouzo effect) is important for advanced oil-recovery processes¹⁵⁵. An example is paraffinic froth treatment in the industrial process of oil sands extraction¹⁵⁶. Heavy oil bitumen with a considerable amount of fine solids and water is separated from oil sands ore by warm-water extraction to form bitumen froth. Solids and water are removed by adding sufficient light alkane (which is a poor solvent for asphaltenes, a solubility family of extremely heavy species of bitumen) to achieve a critical solvent/bitumen ratio. Asphaltene precipitation triggered by this dilution then forms an agglomeration with water drops and solids, sweeping the solids and water off under gravity and producing diluted bitumen of high quality that is easy to transport¹⁵⁷. Control of the size distribution and morphology of asphaltene precipitates may lead to a more efficient oil-recovery approach, with less hydrocarbon loss to waste¹⁵⁵.

Synthetic chemistry and biology. Apart from encapsulation and precursors for nanoparticles as described in the previous subsection, the droplets and their physicochemical hydrodynamics also find many applications in chemical synthesis.

They provide a confined environment in synthetic chemistry to realize cascade reactions in a fashion similar to artificial cells. The surface of microdroplets serves as a biphasic site for catalysts to access immiscible liquid phases inside and outside the droplets, improving the specificity and efficiency of interfacial catalytic reactions for biofuel upgrading¹⁵⁸. The droplets generated from chemical reactions were found to preferentially and differentially segregate and compartmentalize RNA, suggesting that droplets may play a role in protecting essential chemical components for the origin of life¹⁵⁹. Indeed, the droplets can grow and divide from addition of materials produced in droplet reaction, resembling prebiotic protocells^{160–162}.

Microdroplets can also act as microlabs or chemical microreactors, and often chemical reactions that do not take place in bulk water do occur in microdroplets^{163,164}. To account for the enhanced chemical reactions in the microdroplets, a reaction-adsorption mechanism was proposed¹⁶⁵. According to this mechanism, the molecules at the interface are more active, which is attributed to the solvation energy becoming available, owing to solubilization. The energy required for the molecules at the interface to react is therefore less than that in the bulk reaction¹⁶⁵.

Droplets formed from aqueous liquid–liquid phase separation of polyelectrolytes have also drawn interest from biology and cell research. The process of phase separation of an aqueous solution consisting of two oppositely charged polyelectrolytes into two immiscible aqueous phases — coacervate droplets and supernatant — is called coacervation¹⁶⁶. The dense coacervate droplets are rich in polymers, whereas the supernatant is a dilute equilibrium phase, poor in polymers. Coacervation has a long history of use in encapsulation applications¹⁶⁷. The process of coacervation was also proposed as crucial in theories of abiogenesis (the development of life)¹⁶⁸. Coacervation is driven by both entropy and electrostatic interactions between polyelectrolytes, influenced by molecule weight, charge distribution and chirality of polymers, the concentration and the weight ratio of the two polymers and the ionic strength of the aqueous medium. Prior to the macroscopic phase separation, the size distribution of the polyelectrolyte complexes becomes very narrow. Intermolecular complexes of several hundred nanometres form until macroscopic phase separation occurs.

The research interest in this subject has recently intensified owing to the functional

roles of intracellular coacervates and their relation to diseases¹⁶⁹, and owing to the extraordinary properties of coacervates as new materials, namely underwater superglue, bone cement and drug-encapsulating materials, and new processes such as deep tissue bonding or bone fixation, and biological scaffold coatings¹⁷⁰. What remains largely unknown is the evolution of nanoscale coacervates. Model polyelectrolytes with defined molecular weight and charge distribution have been studied to understand the effect of charge patterns¹⁷¹. It would be interesting to quantify the temporal evolution of the coacervate nanocolloids during the phase separation process, to better understand its fluid dynamics.

Inkjet printing. Binary and multicomponent droplets are relevant in inkjet printing^{172–175}, because nearly all inks are multicomponent and not only contain pigments and surfactants, but also consist of various liquids, with different surface tensions, volatilities and viscosities. Moreover, different nozzles of an inkjet printer are operated with different inks. All these features imply that selective evaporation and coalescence of droplets of different liquids as described in the previous section are crucial processes in inkjet printing.

Evaporation and coalescence are important for droplets on the substrate towards which the droplets are jetted, but also for droplets on the nozzle plate of the inkjet channel, close to the nozzle out of which the droplets are jetted, and to the meniscus of the ink itself. Here, selective evaporation of one component of the ink can be a major problem, as we discuss in the context of two examples from piezoelectric inkjet printing¹⁷², which is one of the most advanced and well-controlled forms of inkjet printing:

First, in piezoelectric inkjet printing, the ink in the nozzle is well mixed, thanks to the acoustic field driving the jetting of the droplets. Therefore the material properties of the ink, such as surface tension or viscosity, are determined by the composition of the various liquid components. Now imagine a nozzle at rest for some printing cycles, when that particular ink is not needed. In that time — say, many seconds — one or more components of the ink can selectively evaporate out of the nozzle. This selective evaporation changes the material properties of the remaining ink such as the surface tension and therefore the required pulse strength for jetting once the nozzle is activated again — a major source of inaccuracy.

Second, even worse, droplets of ink on the nozzle plate can selectively evaporate, introducing a concentration gradient and thus surface tension gradient on the nozzle, leading to a Marangoni flow^{176,177}. Once this flow is directed towards the nozzle it can lead to transport of dirt particles into the nozzle, which can lead to air bubble entrainment and nozzle failure^{178,179} — a disaster for the printing process.

Also on the substrate on which the droplets are jetted, Marangoni flow within one droplet^{79,82–92} (FIG. 4a–c) or in between different droplets²⁵ (FIG. 2) can lead to unwanted effects, in particular as these flows transport pigments. However, an open question is whether the emerging Marangoni flow between the droplets perhaps even helps in mixing the droplets ('bleeding of mixed colours'). Another question is how the multicomponent nature of the evaporating droplet and the resulting flows affect the coating pattern^{10,83,173,180,181}. The jetted multicomponent droplets on the substrate may additionally undergo phase changes by evaporation, solidification or chemical reactions. In the latter case of chemical reactions inside the droplets, including reactions leading to solidification, for instance with crosslinkers²⁹, many questions arise. What exactly happens when one reactant diffuses into a droplet of another reactant, for instance from a neighbouring droplet or from some reservoir? How does the reaction propagate from the droplet surface where the two reactants first make contact? And how does a two-component paint 'chemically dry' through crosslinkers? 'Watching paint dry' is in fact interesting, relevant and largely unexplored science. It is also very timely, because of sharpened environmental regulations with respect to the evaporation of (toxic) solvents.

Nanotechnology and materials science.

The solidification process after drop–drop coalescence — with one droplet filled with crosslinkers and the other one with a liquid responsive to it — has been used to manufacture microparticles of controlled shape and size at high rates²⁹. Because the process takes place after collision of such droplets in air (FIG. 2e), it has been called 'in-air microfluidics'. Its control parameters are — next to the droplet sizes and their velocities — the droplet compositions. Through these control parameters, different degrees of Marangoni-flow-driven encapsulation can be achieved, leading to controlled monodisperse emulsions, particles, and fibres with diameters of 20–300 µm.

Additionally, ternary liquids have been used to manufacture microparticles and even nanoparticles, by using the ouzo effect (nanoprecipitation). In fact, with this process, micromaterials and nanomaterials can be built bottom-up in a well-controlled way^{182–184}.

Another important material science application for which the physicochemical hydrodynamics of droplets is relevant is freezing colloids¹⁰³ (FIG. 5b). In this application, the crucial question is how immersed droplets interact with the freezing front in binary or multicomponent freezing liquids. On the one hand, particle-reinforced metal alloys require homogeneous distribution of particles in the matrix, and an immediate engulfment is therefore preferred. On the other hand, for single-crystal growth, a complete rejection of impurities is crucial^{104,185}. A rejection is also preferred whenever engulfed droplets or bubbles would introduce uncontrolled defects into a cooling alloy.

Finally, a very important application of the physicochemical hydrodynamics of droplets is in the semiconductor industry and in nanotechnology, for which surfaces such as wafers must be extremely clean and dry. This can be achieved by 'Marangoni drying'^{85,186–190}, in which gradients in surface tension are imposed to drive the liquid of a thin film outwards, for instance through local vapour deposition of a different fluid (often isopropyl alcohol), which absorbs on the film, or through deposition of a multicomponent droplet⁹⁹. For Marangoni drying to work properly, the interaction of sessile droplets on the wafer is essential, and unexpected hindrance of coalescence of droplets of different liquids, as shown in REFS^{25,26} (FIG. 2a), is a major problem.

In the context of drying wafers with their nanoscale structures, capillary forces can also cause problems¹⁹¹. When a sessile droplet attached to different structures on a surface is evaporating, the capillary forces, which are tremendous on the tiny length scales relevant on wafers, pull these structures together, and this can break them^{192–194}.

Outlook and general lessons

Much remains to be done, from a fundamental point of view, but also from the application side. New applications that are relevant for society of the physicochemical hydrodynamics of droplets far from equilibrium are popping up at a high rate. But we expect that the rapid progress in this field will continue, as from our point of view we are living in the golden age of fluid dynamics. The continuous increase in computational power means that

simulations that we did not dare to dream of even 10 years ago are now possible. A similar revolution (for the same reason) is taking place in digital high-speed imaging, thanks to which one can now routinely resolve the millisecond timescale and below, revealing new physics on these scales, which up to now was inaccessible, and producing a huge amount of data on the flow. Moreover, other advanced equipment such as confocal microscopy, digital holographic microscopy and atomic force microscopy is coming to be used more and more in fluid dynamics. Considering all of these advances together, the gap between what can be measured and what can be simulated ab initio is narrowing more quickly than we had anticipated at the end of the last century. Other gaps are also closing. Fluid dynamics is bridging out into neighbouring disciplines, such as chemistry, and in particular colloid science, chemical analysis and diagnostics, lab-on-a-chip microfluidics, catalysis, electrolysis, medicine, biology, computational and data science, among many others. Here, the techniques, approaches and traditions from fluid dynamics can offer a great deal of help to solve outstanding problems. Vice versa, these fields can offer wonderful questions to fluid dynamics.

In our opinion, anyone who has dismissed experiments with tears of wine, or with coffee, whisky or ouzo drops, as a gimmick is very much mistaken. On the one hand, as discussed above, important physics, chemistry, fluid dynamics and colloid and materials science can be learned from these systems and processes, with many modern applications in diagnostics, pharmaceuticals, biology, medicine, chemical and environmental engineering, inkjet printing, nanotechnology and micro-manufacturing, all of huge relevance. On the other hand — and here we come to the education in science, which may be even more important than any application — the deciphering of these everyday phenomena offers examples par excellence of the physicist's approach: first translate an observed phenomenon into a clean experiment with well-defined control parameters, then make precise observations and record data, then develop a theory and a model and confirm these by calculations and numerical simulations, and finally make predictions about how the system will behave with values for the control parameters from an even wider range. Studying the fluid physics of these everyday systems is therefore also very suitable for the conceptual training of doctoral students, who can learn in this way, simultaneously and by example, clean experimentation,

theory formulation, modelling and numerical simulation, which from our point of view is much more motivating and broader than being a small cog for a specific detail of a large-scale experiment with thousands of scientists involved.

Detlef Lohse^{1,2} and Xuehua Zhang^{1,3}

¹Physics of Fluids Group, Max Planck Center for Complex Fluid Dynamics, MESA+ Research Institute and J. M. Burgers Centre for Fluid Dynamics, University of Twente, Enschede, The Netherlands.

²Max Planck Institute for Dynamics and Self-Organization, Göttingen, Germany.

³Department of Chemical and Materials Engineering, University of Alberta, Edmonton, Alberta, Canada.

[✉]e-mail: d.lohse@utwente.nl; xuehua.zhang@ualberta.ca

<https://doi.org/10.1038/s42254-020-0199-z>

Published online 23 July 2020

- Levich, V. G. *Physicochemical Hydrodynamics* (Prentice Hall, 1962).
- Cates, M. E. & Tjhung, E. Theories of binary fluid mixtures: from phase-separation kinetics to active emulsions. *J. Fluid Mech.* **836**, <https://doi.org/10.1017/jfm.2017.832> (2018).
- Lauga, E. & Powers, T. R. The hydrodynamics of swimming microorganisms. *Rep. Prog. Phys.* **72**, 096601 (2009).
- Maass, C. C., Krüger, C., Herminghaus, S. & Bahr, C. Swimming droplets. *Annu. Rev. Cond. Matter Phys.* **7**, 171–193 (2016).
- Moran, J. L. & Posner, J. D. Phoretic self-propulsion. *Annu. Rev. Fluid Mech.* **49**, 511–540 (2017).
- Golestanian, R. Phoretic active matter. Preprint at <https://arxiv.org/abs/1909.03747> (2019).
- Manikantan, H. & Squires, T. M. Surfactant dynamics: hidden variables controlling fluid flows. *J. Fluid Mech.* **892** <https://doi.org/10.1017/jfm.2020.170> (2020).
- Cazabat, A. M. & Guéna, G. Evaporation of macroscopic sessile droplets. *Soft Matter* **6**, 2591–2612 (2010).
- Erbil, H. Y. Evaporation of pure liquid sessile and spherical suspended drops: a review. *Adv. Colloid Interface Sci.* **170**, 67–86 (2012).
- Sefiane, K. Patterns from drying drops. *Adv. Colloid Interface Sci.* **206**, 372–381 (2014).
- Lohse, D. & Zhang, X. Surface nanobubble and surface nanodroplets. *Rev. Mod. Phys.* **87**, 981–1035 (2015).
- Jain, A. & Verma, K. K. Recent advances in applications of single-drop microextraction: a review. *Anal. Chim. Acta* **706**, 37–65 (2011).
- de Wit, A. Chemo-hydrodynamic patterns and instabilities. *Annu. Rev. Fluid Mech.* **52**, 531–555 (2020).
- Lohse, D. Bubble puzzles: from fundamentals to applications. *Phys. Rev. Fluids* **3**, 110504 (2018).
- Young, N., Goldstein, J. & Block, M. J. The motion of bubbles in a vertical temperature gradient. *J. Fluid Mech.* **6**, 350–356 (1959).
- Li, Y. et al. Bouncing oil droplet in a stratified liquid and its sudden death. *Phys. Rev. Lett.* **122**, 154502 (2019).
- Anderson, J. L. Colloid transport by interfacial forces. *Annu. Rev. Fluid Mech.* **21**, 61–99 (1989).
- Anderson, J. L., Lowell, M. E. & Prieve, D. C. Motion of a particle generated by chemical gradients. Part 1. Non-electrolytes. *J. Fluid Mech.* **117**, 107–121 (1982).
- Izri, Z., Van Der Linden, M. N., Michelin, S. & Dauchot, O. Self-propulsion of pure water droplets by spontaneous Marangoni-stress-driven motion. *Phys. Rev. Lett.* **113**, 248302 (2014).
- Marbach, S., Yoshida, H. & Bocquet, L. Osmotic and diffusio-osmotic flow generation at high solute concentration. I. Mechanical approaches. *J. Chem. Phys.* **146**, 194701 (2017).
- Prieve, D. C., Malone, S. M., Khair, A. S., Stout, R. F. & Kanj, M. Y. Diffusiophoresis of charged colloidal particles in the limit of very high salinity. *Proc. Natl Acad. Sci. USA* **116**, 18257–18262 (2019).
- Yang, F., Shin, S. & Stone, H. A. Diffusiophoresis of a charged drop. *J. Fluid Mech.* **852**, 37–59 (2018).
- Morozov, M. & Michelin, S. Nonlinear dynamics of a chemically-active drop: from steady to chaotic self-propulsion. *J. Chem. Phys.* **150**, 044110 (2019).
- Riegler, H. & Lazar, P. Delayed coalescence behavior of droplets with completely miscible liquids. *Langmuir* **24**, 6395–6398 (2008).
- Karpitschka, S. & Riegler, H. Quantitative experimental study on the transition between fast and delayed coalescence of sessile droplets with different but completely miscible liquids. *Langmuir* **26**, 11825–11829 (2010).
- Karpitschka, S. & Riegler, H. Noncoalescence of sessile drops from different but miscible liquids: hydrodynamic analysis of the twin drop contour as a self-stabilizing traveling wave. *Phys. Rev. Lett.* **109**, 066103 (2012).
- Koldewei, R. B., Van Capelleveen, B. F., Lohse, D. & Visser, C. W. Marangoni-driven spreading of miscible liquids in the binary pendant drop geometry. *Soft Matter* **15**, 8525–8531 (2019).
- Yeo, Y., Basaran, O. A. & Park, K. A new process for making reservoir-type microcapsules using ink-jet technology and interfacial phase separation. *J. Control. Release* **93**, 161–173 (2003).
- Visser, C. W., Kamperman, T., Karbaat, L. P., Lohse, D. & Karperien, M. In-air microfluidics enables rapid fabrication of emulsions, suspensions, and 3D modular (bio) materials. *Sci. Adv.* **4**, ea01175 (2018).
- Yu, H., Kant, P., Dyett, B., Lohse, D. & Zhang, X. Splitting droplet through coalescence of two different three-phase contact lines. *Soft Matter* **15**, 6055–6061 (2019).
- Berg, S. Marangoni-driven spreading along liquid-liquid interfaces. *Phys. Fluids* **21**, 032105 (2009).
- Wodlfe, F., Sebilliau, J., Magnaudet, J. & Pimienta, V. Marangoni-driven flower-like patterning of an evaporating drop spreading on a liquid substrate. *Nat. Commun.* **9**, 820 (2018).
- Jehannin, M. et al. Periodic precipitation patterns during coalescence of reacting sessile droplets. *Langmuir* **31**, 11484–11490 (2015).
- Paxton, W. et al. Catalytic nanomotors: autonomous movement of striped nanorods. *J. Am. Chem. Soc.* **126**, 13424–13431 (2004).
- Golestanian, R., Liverpool, T. B. & Ajdari, A. Propulsion of a molecular machine by asymmetric distribution of reaction products. *Phys. Rev. Lett.* **94**, 220801 (2005).
- Jiang, H.-R., Yoshinaga, N. & Sano, M. Active motion of a Janus particle by self-thermophoresis in a defocused laser beam. *Phys. Rev. Lett.* **105**, 268302 (2010).
- Buttinoni, I. et al. Dynamical clustering and phase separation in suspensions of self-propelled colloidal particles. *Phys. Rev. Lett.* **110**, 238301 (2013).
- Michelin, S. & Lauga, E. Phoretic self-propulsion at finite Péclet numbers. *J. Fluid Mech.* **747**, 572–604 (2014).
- Michelin, S., Lauga, E. & Bartolo, D. Spontaneous autophoretic motion of isotropic particles. *Phys. Fluids* **25**, 061701 (2013).
- Golovin, A., Gupalo, Y. P. & Ryazantsev, Y. S. Change in shape of drop moving due to the chemistromocapillary effect. *J. Appl. Mech. Tech. Phys.* **30**, 602–609 (1989).
- Rednikov, A. Y., Ryazantsev, Y. S. & Velarde, M. G. Drop motion with surfactant transfer in a homogeneous surrounding. *Phys. Fluids* **6**, 451–468 (1994).
- Schmitt, M. & Stark, H. Swimming active droplet: a theoretical analysis. *EPL* **101**, 44008 (2013).
- Morozov, M. & Michelin, S. Self-propulsion near the onset of Marangoni instability of deformable active droplets. *J. Fluid Mech.* **860**, 711–738 (2019).
- Abécassis, B., Cottin-Bizonne, C., Ybert, C., Ajdari, A. & Bocquet, L. Boosting migration of large particles by solute contrasts. *Nat. Mater.* **7**, 785–789 (2008).
- Palacci, J., Abécassis, B., Cottin-Bizonne, C., Ybert, C. & Bocquet, L. Colloidal motility and pattern formation under rectified diffusiophoresis. *Phys. Rev. Lett.* **104**, 138302 (2010).
- Banerjee, A., Williams, I., Azevedo, R. N., Helgeson, M. E. & Squires, T. M. Solutio-inertial phenomena: designing long-range, long-lasting, surface-specific interactions in suspensions. *Proc. Natl Acad. Sci. USA* **113**, 8612–8617 (2016).
- Banerjee, A. & Squires, T. M. Long-range, selective, on-demand suspension interactions: combining and triggering soluto-inertial beacons. *Sci. Adv.* **5**, eaax1893 (2019).
- Krüger, C., Klöds, G., Bahr, C. & Maass, C. C. Curling liquid crystal microswimmers: a cascade of spontaneous symmetry breaking. *Phys. Rev. Lett.* **117**, 048003 (2016).
- Suga, M., Suda, S., Ichikawa, M. & Kimura, Y. Self-propelled motion switching in nematic liquid crystal droplets in aqueous surfactant solutions. *Phys. Rev. E* **97**, 062703 (2018).

50. Hu, W.-F., Lin, T.-S., Rafai, S. & Misbah, C. Chaotic swimming of phoretic particles. *Phys. Rev. Lett.* **123**, 238004 (2019).
51. Thutupalli, S., Seemann, R. & Herminghaus, S. Swarming behavior of simple model squirmers. *New J. Phys.* **13**, 073021 (2011).
52. Palacci, J., Sacanna, S., Steinberg, A. P., Pine, D. J. & Chaikin, P. M. Living crystals of light-actuated colloidal surfers. *Science* **359**, 936–940 (2013).
53. Moerman, P. G. et al. Solute-mediated interactions between active droplets. *Phys. Rev. E* **96**, 032607 (2017).
54. Lippera, K., Morozov, M., Benzaquen, M. & Michelin, S. Collisions and rebounds of chemically-active droplets. *J. Fluid Mech.* **886**, A17 (2020).
55. Peña, A. A. & Miller, C. A. Solubilization rates of oils in surfactant solutions and their relationship to mass transport in emulsions. *Adv. Colloid Interface Sci.* **123**, 241–257 (2006).
56. Herminghaus, S. et al. Interfacial mechanisms in active emulsions. *Soft Matter* **10**, 7008–7022 (2014).
57. Hokmabad, B. V., Baldwin, K. A., Krüger, C., Bahr, C. & Maass, C. C. Topological stabilization and dynamics of self-propelling nematic shells. *Phys. Rev. Lett.* **123**, 178003 (2019).
58. Poesio, P., Beretta, G. P. & Thorsen, T. Dissolution of a liquid microdroplet in a nonideal liquid–liquid mixture far from thermodynamic equilibrium. *Phys. Rev. Lett.* **103**, 064501 (2009).
59. Lagzi, I., Soh, S., Wesson, P. J., Browne, K. P. & Grzybowski, B. A. Maze solving by chemotactic droplets. *J. Am. Chem. Soc.* **132**, 1198–1199 (2010).
60. Cejkova, J., Novak, M., Stepanek, F. & Hanczyc, M. M. Dynamics of chemotactic droplets in salt concentration gradients. *Langmuir* **30**, 11937–11944 (2014).
61. Jin, C., Krüger, C. & Maass, C. C. Chemotaxis and autochemotaxis of self-propelling droplet swimmers. *Proc. Natl Acad. Sci. USA* **114**, 5089–5094 (2017).
62. Epstein, P. S. & Plesset, M. S. On the stability of gas bubbles in liquid–gas solutions. *J. Chem. Phys.* **18**, 1505–1509 (1950).
63. Duncan, P. B. & Needham, D. Microdroplet dissolution into a second-phase solvent using a micropipet technique: test of the Epstein–Plesset model for an aniline–water system. *Langmuir* **22**, 4190–4197 (2006).
64. Picknett, R. G. & Bexon, R. The evaporation of sessile or pendant drops in still air. *J. Colloid Interface Sci.* **61**, 336–350 (1977).
65. Deegan, R. D. et al. Capillary flow as the cause of ring stains from dried liquid drops. *Nature* **389**, 827–829 (1997).
66. Hu, H. & Larson, R. G. Evaporation of a sessile droplet on a substrate. *J. Phys. Chem. B* **106**, 1354 (2002).
67. Popov, Y. O. Evaporative deposition patterns: spatial dimensions of the deposit. *Phys. Rev. E* **71**, 036313 (2005).
68. Gelderblom, H. et al. How water droplets evaporate on a superhydrophobic substrate. *Phys. Rev. E* **83**, 026306 (2011).
69. Stauber, J. M., Wilson, S. K., Duffy, B. R. & Sefiane, K. On the lifetimes of evaporating droplets. *J. Fluid Mech.* **744**, R2 (2014).
70. Dietrich, E. et al. Role of natural convection in the dissolution of sessile droplets. *J. Fluid Mech.* **794**, 45–67 (2016).
71. Laghezza, G. et al. Collective and convective effects compete in patterns of dissolving surface droplets. *Soft Matter* **12**, 5787–5796 (2016).
72. Carrier, O. et al. Evaporation of water: evaporation rate and collective effects. *J. Fluid Mech.* **798**, 774–786 (2016).
73. Zhu, X., Verzicco, R., Zhang, X. & Lohse, D. Diffusive interaction of multiple surface nanobubbles: shrinkage, growth, and coarsening. *Soft Matter* **14**, 2006–2014 (2018).
74. Michelin, S., Guérin, E. & Lauga, E. Collective dissolution of microbubbles. *Phys. Rev. Fluids* **3**, 043601 (2018).
75. Bao, L. et al. Flow-induced dissolution of femtoliter surface droplet arrays. *Lab Chip* **18**, 1066–1074 (2018).
76. Wray, A. W., Duffy, B. R. & Wilson, S. K. Competitive evaporation of multiple sessile droplets. *J. Fluid Mech.* **884**, A45 (2020).
77. Chong, K. L., Li, Y., Ng, C. S., Verzicco, R. & Lohse, D. Convection-dominated dissolution for single and multiple immersed sessile droplets. *J. Fluid Mech.* **892**, A21 (2020).
78. Deegan, R. D. et al. Contact line deposits in an evaporating drop. *Phys. Rev. E* **62**, 756–765 (1998).
79. Scriven, L. & Sternling, C. The Marangoni effects. *Nature* **187**, 186–188 (1960).
80. Hu, H. & Larson, R. G. Analysis of the effects of Marangoni stresses on the microflow in an evaporating sessile droplet. *Langmuir* **21**, 3972–3980 (2005).
81. Bennacer, R. & Sefiane, K. Vortices, dissipation and flow transition in volatile binary drops. *J. Fluid Mech.* **749**, 649–665 (2014).
82. Tan, H. et al. Evaporation-triggered microdroplet nucleation and the four life phases of an evaporating ouzo drop. *Proc. Natl Acad. Sci. USA* **113**, 8642–8647 (2016).
83. Kim, H. et al. Controlled uniform coating from the interplay of Marangoni flows and surface-adsorbed macromolecules. *Phys. Rev. Lett.* **116**, 124501 (2016).
84. Dietrich, E. et al. Segregation in dissolving binary component sessile droplets. *J. Fluid Mech.* **812**, 349–369 (2017).
85. Karpitschka, S., Liebig, F. & Riegler, H. Marangoni contraction of evaporating sessile droplets of binary mixtures. *Langmuir* **33**, 4682–4687 (2017).
86. Diddens, C. et al. Evaporating pure, binary and ternary droplets: thermal effects and axial symmetry breaking. *J. Fluid Mech.* **823**, 470–497 (2017).
87. Kim, H., Müller, K., Shardt, O., Afkhami, S. & Stone, H. A. Solutal Marangoni flows of miscible liquids drive transport without surface contamination. *Nat. Phys.* **13**, 1105 (2017).
88. Li, Y. et al. Evaporation-triggered segregation of sessile binary droplets. *Phys. Rev. Lett.* **120**, 224501 (2018).
89. Kim, H. & Stone, H. A. Direct measurement of selective evaporation of binary mixture droplets by dissolving materials. *J. Fluid Mech.* **850**, 769–783 (2018).
90. Edwards, A. et al. Density-driven flows in evaporating binary liquid droplets. *Phys. Rev. Lett.* **121**, 184501 (2018).
91. Li, Y. et al. Gravitational effect in evaporating binary microdroplets. *Phys. Rev. Lett.* **122**, 114501 (2019).
92. Marin, A. et al. Solutal Marangoni flow as the cause of ring stains from drying salty colloidal drops. *Phys. Rev. Fluids* **4**, 041601 (2019).
93. Hosoi, A. E. & Bush, J. W. M. Evaporative instabilities in climbing films. *J. Fluid Mech.* **442**, 217–239 (2001).
94. Shin, S., Jacobi, I. & Stone, H. A. Bénard–Marangoni instability driven by moisture absorption. *EPL* **113**, 24002 (2016).
95. Karpitschka, S. The value of a fading tracer. *J. Fluid Mech.* **856**, 1–4 (2018).
96. Li, Y. et al. Rayleigh–Taylor instability by segregation in an evaporating multicomponent microdroplet. *J. Fluid Mech.* in the press.
97. Keiser, L., Bense, H., Colinet, P., Bico, J. & Reyssat, E. Marangoni bursting: evaporation-induced emulsification of binary mixtures on a liquid layer. *Phys. Rev. Lett.* **118**, 074504 (2017).
98. Durey, G. et al. Marangoni bursting: evaporation-induced emulsification of a two-component droplet. *Phys. Rev. Fluids* **3**, 100501 (2018).
99. Hernández-Sánchez, J. F., Eddi, A. & Snoeijer, J. H. Marangoni spreading due to a localized alcohol supply on a thin water film. *Phys. Fluids* **27**, 032003 (2015).
100. Maheshwari, S., Van Der Hoef, M., Prosperetti, A. & Lohse, D. Molecular dynamics study of multicomponent droplet dissolution in a sparingly miscible liquid. *J. Fluid Mech.* **833**, 54–69 (2017).
101. Chu, S. & Prosperetti, A. Dissolution and growth of a multicomponent drop in an immiscible liquid. *J. Fluid Mech.* **798**, 787–811 (2016).
102. Lohse, D. Towards controlled liquid–liquid microextraction. *J. Fluid Mech.* **804**, 1–4 (2016).
103. Deville, S. *Freezing Colloids: Observations, Principles, Control, and Use. Applications in Materials Science, Life Science, Earth Science, Food Science, and Engineering* (Springer, 2017).
104. Dedovets, D., Montoux, C. & Deville, S. Five-dimensional imaging of freezing emulsions with solute effects. *Science* **360**, 303–306 (2018).
105. Vitale, S. & Katz, J. Liquid droplet dispersions formed by homogeneous liquid–liquid nucleation: ‘the ouzo effect’. *Langmuir* **19**, 4105–4110 (2003).
106. Ganachaud, F. & Katz, J. Nanoparticles and nanocapsules created using the ouzo effect: spontaneous emulsification as an alternative to ultrasonic and high-shear devices. *Chem. Phys. Chem* **6**, 209–216 (2005).
107. Lepeltier, E., Bourgaux, C. & Couvreur, P. Nanoprecipitation and the ‘ouzo effect’: application to drug delivery devices. *Adv. Drug Deliv. Rev.* **71**, 86–97 (2014).
108. Voorhees, P. W. The theory of Ostwald ripening. *J. Stat. Phys.* **38**, 231–252 (1985).
109. Solans, C., Izquierdo, P., Nolla, J., Azemar, N. & Garcia-Celma, M. J. Nano-emulsions. *Curr. Opin. Colloid Interface Sci.* **10**, 102–110 (2005).
110. Zemb, T. N. et al. How to explain microemulsions formed by solvent mixtures without conventional surfactants. *Proc. Natl Acad. Sci. USA* **113**, 4260–4265 (2016).
111. Zhang, X. H. et al. From transient nanodroplets to permanent nanolenses. *Soft Matter* **8**, 4314–4317 (2012).
112. Joanny, J. & de Gennes, P. A model for contact angle hysteresis. *J. Chem. Phys.* **81**, 552 (1984).
113. de Gennes, P. G. Wetting: statics and dynamics. *Rev. Mod. Phys.* **57**, 827–863 (1985).
114. Liu, Y. & Zhang, X. Evaporation dynamics of nanodroplets and their anomalous stability on rough substrates. *Phys. Rev. E* **88**, 012404 (2013).
115. Lohse, D. & Zhang, X. Pinning and gas oversaturation imply stable single surface nanobubble. *Phys. Rev. E* **91**, 031003(R) (2015).
116. Zhang, X. et al. Formation of surface nanodroplets under controlled flow conditions. *Proc. Natl Acad. Sci. USA* **112**, 9253–9257 (2015).
117. Yu, H., Lu, Z., Lohse, D. & Zhang, X. Gravitational effect on the formation of surface nanodroplets. *Langmuir* **31**, 12628–12634 (2015).
118. Yu, H., Maheshwari, S., Zhu, J., Lohse, D. & Zhang, X. Formation of surface nanodroplets facing a structured microchannel wall. *Lab Chip* **17**, 1496–1504 (2017).
119. Zeng, B., Wang, Y., Zhang, X. & Lohse, D. Solvent exchange in a Hele–Shaw cell: universality of surface nanodroplet nucleation. *J. Phys. Chem. C* **123**, 5571–5577 (2019).
120. Bao, L., Werbiuk, Z., Lohse, D. & Zhang, Z. Controlling the growth modes of femtoliter sessile droplets nucleating on chemically patterned surfaces. *J. Phys. Chem. Lett.* **7**, 1055–1059 (2016).
121. Peng, S., Mega, T. L. & Zhang, X. Collective effects in microbubble growth by solvent exchange. *Langmuir* **32**, 11265–11272 (2016).
122. Dyett, B. et al. Growth dynamics of surface nanodroplets during solvent exchange at varying flow rates. *Soft Matter* **14**, 5197 (2018).
123. Peng, S., Lohse, D. & Zhang, X. Spontaneous pattern formation of surface nanodroplets from competitive growth. *ACS Nano* **9**, 11916–11923 (2015).
124. Xu, C. et al. Collective interactions in the nucleation and growth of surface droplets. *Soft Matter* **13**, 937–944 (2017).
125. Dyett, B., Hao, H., Lohse, D. & Zhang, X. Coalescence driven self-organization of growing nanodroplets around a microcap. *Soft Matter* **14**, 2628–2637 (2018).
126. Schlichting, H. *Boundary Layer Theory* 7th edn (McGraw Hill, 1979).
127. Zhang, X. et al. Mixed mode of dissolving immersed microdroplets at a solid–water interface. *Soft Matter* **11**, 1889–1900 (2015).
128. Tan, H. et al. Self-wrapping of an ouzo drop induced by evaporation on a superamphiphobic surface. *Soft Matter* **13**, 2749–2759 (2017).
129. Tan, H. et al. Microdroplet nucleation by dissolution of a multicomponent drop in a host liquid. *J. Fluid Mech.* **870**, 217–246 (2019).
130. Kirkaldy, J. S. & Brown, L. Diffusion behaviour in ternary, multiphase systems. *Can. Metall. Q.* **2**, 89–115 (1963).
131. Ruschak, K. J. & Miller, C. A. Spontaneous emulsification in ternary systems with mass transfer. *Ind. Eng. Chem. Fundamentals* **11**, 534–540 (1972).
132. Miller, C. A., Neogi, P. *Interfacial Phenomena: Equilibrium and Dynamic Effects* Vol. 139 (CRC, 2007).
133. Otero, J., Meeker, S. & Clegg, P. S. Compositional ripening of particle-stabilized drops in a three-liquid system. *Soft Matter* **14**, 3783–3790 (2018).
134. Choi, C.-H., Weitz, D. A. & Lee, C.-S. One step formation of controllable complex emulsions: from functional particles to simultaneous encapsulation of hydrophilic and hydrophobic agents into desired position. *Adv. Mater.* **25**, 2536–2541 (2013).
135. Haase, M. F. & Bruijic, J. Tailoring of high-order multiple emulsions by the liquid–liquid phase separation of ternary mixtures. *Angew. Chemie Int. Ed.* **53**, 11793–11797 (2014).
136. Zarzar, L. D. et al. Dynamically reconfigurable complex emulsions via tunable interfacial tensions. *Nature* **518**, 520 (2015).

137. Lopian, T. et al. Morphologies observed in ultraflexible microemulsions with and without the presence of a strong acid. *ACS Cent. Sci.* **2**, 467–475 (2016).
138. Lu, Z. et al. Universal nanodroplet branches from confining the ouzo effect. *Proc. Natl Acad. Sci. USA* **114**, 10332–10337 (2017).
139. Moerman, P. G., Hohenberg, P. C., Vanden-Eijnden, E. & Bruijic, J. Emulsion patterns in the wake of a liquid–liquid phase separation front. *Proc. Natl Acad. Sci. USA* **115**, 3599–3604 (2018).
140. Hajian, R. & Hardt, S. Formation and lateral migration of nanodroplets via solvent shifting in a microfluidic device. *Microfluid. Nanofluidics* **19**, 1281–1296 (2015).
141. Pregl, F. *Die quantitative organische Mikroanalyse* (Springer, 1917).
142. Rezaee, M. et al. Determination of organic compounds in water using dispersive liquid–liquid microextraction. *J. Chromatogr. A* **1116**, 1–9 (2006).
143. Rezaee, M., Yamini, Y. & Faraji, M. Evolution of dispersive liquid–liquid microextraction method. *J. Chromatogr. A* **1217**, 2342–2357 (2010).
144. Zgola-Grzeskowiak, A. & Grzeskowiak, T. Dispersive liquid–liquid microextraction. *Trends Anal. Chem.* **30**, 1382–1399 (2011).
145. Gutiérrez, J. M. P., Hinkley, T., Taylor, J. W., Yanev, K. & Cronin, L. Evolution of oil droplets in a chemorobotic platform. *Nat. Commun.* **5**, 5571 (2014).
146. Ocaña-González, J. A., Fernández-Torres, R., Bello-López, M. A. & Ramos-Payán, M. New developments in microextraction techniques in bioanalysis. A review. *Anal. Chim. Acta* **905**, 8–23 (2016).
147. Li, M., Dyett, B., Yu, H., Bansal, V. & Zhang, X. Functional femtoliter droplets for ultrafast nanoextraction and supersensitive online microanalysis. *Small* **15**, 1804683 (2019).
148. Li, M., Dyett, B. & Zhang, X. Automated femtoliter droplet-based determination of oil–water partition coefficient. *Anal. Chem.* **91**, 10371–10375 (2019).
149. Qian, J. et al. One-step nanoextraction and ultrafast microanalysis based on nanodroplet formation in an evaporating ternary liquid microfilm. *Adv. Mater. Technol.* **5**, 1900740 (2020).
150. Gutiérrez, J. et al. Nano-emulsions: new applications and optimization of their preparation. *Curr. Opin. Colloid Interface Sci.* **13**, 245–251 (2008).
151. Zhang, C., Pansare, V. J., Prud'homme, R. K. & Priestley, R. D. Flash nanoprecipitation of polystyrene nanoparticles. *Soft Matter* **8**, 86–93 (2012).
152. Akbulut, M. et al. Generic method of preparing multifunctional fluorescent nanoparticles using flash nanoprecipitation. *Adv. Funct. Mater.* **19**, 718–725 (2009).
153. Zeng, Z. et al. Scalable production of therapeutic protein nanoparticles using flash nanoprecipitation. *Adv. Healthc. Mater.* **8**, 1801010 (2019).
154. Coquerel, G. Crystallization of molecular systems from solution: phase diagrams, supersaturation and other basic concepts. *Chem. Soc. Rev.* **43**, 2286–2300 (2014).
155. Sun, X., Zhang, Y., Chen, G. & Gai, Z. Application of nanoparticles in enhanced oil recovery: a critical review of recent progress. *Energies* **10**, 345 (2017).
156. Rao, F. & Liu, Q. Froth treatment in Athabasca oil sands bitumen recovery process: a review. *Energy Fuels* **27**, 7199–7207 (2013).
157. He, L., Lin, F., Li, X., Sui, H. & Xu, Z. Interfacial sciences in unconventional petroleum production: from fundamentals to applications. *Chem. Soc. Rev.* **44**, 5446–5494 (2015).
158. Crossley, S., Faria, J., Shen, M. & Resasco, D. E. Solid nanoparticles that catalyze biofuel upgrade reactions at the water/oil interface. *Science* **327**, 68–72 (2010).
159. Jia, T. Z. et al. Membraneless polyester microdroplets as primordial compartments at the origins of life. *Proc. Natl Acad. Sci. USA* **116**, 15830–15835 (2019).
160. Zwicker, D., Decker, M., Jaensch, S., Hyman, A. A. & Jülicher, F. Centrosomes are autocatalytic droplets of pericentriolar material organized by centrioles. *Proc. Natl Acad. Sci. USA* **111**, 2636–2645 (2014).
161. Zwicker, D., Seybold, R., Weber, C. A., Hyman, A. A. & Jülicher, F. Growth and division of active droplets provides a model for protocells. *Nat. Phys.* **13**, 408 (2017).
162. Golestanian, R. Division for multiplication. *Nat. Phys.* **13**, 323–324 (2017).
163. Lee, J. K., Kim, S., Nam, H. G. & Zare, R. N. Microdroplet fusion mass spectrometry for fast reaction kinetics. *Proc. Natl Acad. Sci. USA* **112**, 3898–3903 (2015).
164. Lee, J. K., Samanta, D., Nam, H. G. & Zare, R. N. Micrometer-sized water droplets induce spontaneous reduction. *J. Am. Chem. Soc.* **141**, 10585–10589 (2019).
165. Fallah-Araghi, A. et al. Enhanced chemical synthesis at soft interfaces: a universal reaction–adsorption mechanism in microcompartments. *Phys. Rev. Lett.* **112**, 028301 (2014).
166. Overbeek, J. T. G. & Voorn, M. J. Phase separation in polyelectrolyte solutions. Theory of complex coacervation. *J. Cell. Comp. Physiol.* **49**, 7–26 (1957).
167. Kizilay, E., Kayitmazer, A. & Dubin, P. Complexation and coacervation of polyelectrolytes with oppositely charged colloids. *Adv. Colloid Interface Sci.* **167**, 24–37 (2011).
168. Oparin, A. I. et al. *The Origin of Life on the Earth* (Oliver & Boyd, 1957).
169. Shin, Y. & Brangwynne, C. P. Liquid phase condensation in cell physiology and disease. *Science* **357**, eaaf4382 (2017).
170. Seo, S. et al. Microphase behavior and enhanced wet-cohesion of synthetic copolyampholytes inspired by a mussel foot protein. *J. Am. Chem. Soc.* **137**, 9214–9217 (2015).
171. Chang, L.-W. et al. Sequence and entropy-based control of complex coacervates. *Nat. Commun.* **8**, 1273 (2017).
172. Wijshoff, H. The dynamics of the piezo inkjet printhead operation. *Phys. Rep.* **491**, 77–177 (2010).
173. Kuang, M., Wang, L. & Song, Y. Controllable printing droplets for high-resolution patterns. *Adv. Mater.* **26**, 6950–6958 (2014).
174. Hoath, S. D. *Fundamentals of Inkjet Printing: The Science of Inkjet and Droplets* (Wiley, 2016).
175. Dijkstra, J. F. *Design of Piezo Inkjet Print Heads: From Acoustics to Applications* (Wiley, 2019).
176. de Jong, J. et al. Marangoni flow on an inkjet nozzle plate. *Appl. Phys. Lett.* **91**, 204102 (2007).
177. Beulen, B. et al. Flows on the nozzle plate of an inkjet printhead. *Exp. Fluids* **42**, 217–224 (2007).
178. de Jong, J. et al. Entrapped air bubbles in piezo-driven inkjet printing: their effect on the droplet velocity. *Phys. Fluids* **18**, 121511 (2006).
179. Fraters, A. et al. Inkjet nozzle failure by heterogeneous nucleation: bubble entrainment, cavitation, and diffusive growth. *Phys. Rev. Appl.* **12**, 064019 (2019).
180. Han, W. & Lin, Z. Learning from ‘coffee rings’: ordered structures enabled by controlled evaporative self-assembly. *Angew. Chemie Int. Ed.* **51**, 1534–1546 (2012).
181. Cai, Y. & Zhang-Newby, B.-m. Marangoni flow-induced self-assembly of hexagonal and stripe-like nanoparticle patterns. *J. Am. Chem. Soc.* **130**, 6076–6077 (2008).
182. Reverchon, E., De Marco, I. & Torino, E. Nanoparticles production by supercritical antisolvent precipitation: a general interpretation. *J. Supercrit. Fluids* **43**, 126–138 (2007).
183. Chan, H.-K. & Kwok, P. C. L. Production methods for nanodrug particles using the bottom-up approach. *Adv. Drug Deliv. Rev.* **63**, 406–416 (2011).
184. Huang, W. & Zhang, C. Tuning the size of poly(lactic-co-glycolic acid) (PLGA) nanoparticles fabricated by nanoprecipitation. *Biotechnol. J.* **13**, 1700203 (2018).
185. Zhang, L.-f. Indirect methods of detecting and evaluating inclusions in steel: a review. *J. Iron Steel Res. Int.* **13**, 1–8 (2006).
186. Leenaars, A., Huethorst, J. & Van Oekel, J. Marangoni drying: a new extremely clean drying process. *Langmuir* **6**, 1701–1703 (1990).
187. Marra, J. & Huethorst, J. Physical principles of Marangoni drying. *Langmuir* **7**, 2748–2755 (1991).
188. O'Brien, S. On marangoni drying: nonlinear kinematic waves in a thin film. *J. Fluid Mech.* **254**, 649–670 (1993).
189. Thess, A. & Boos, W. A model for Marangoni drying. *Phys. Fluids* **11**, 3852–3855 (1999).
190. Matar, O. & Craster, R. Models for Marangoni drying. *Phys. Fluids* **13**, 1869–1883 (2001).
191. Okorn-Schmidt, H. F. et al. Particle cleaning technologies to meet advanced semiconductor device process requirements. *ECS J. Solid State Sci. Technol.* **3**, N3069–N3080 (2014).
192. Bico, J., Roman, B., Moulin, L. & Boudaoud, A. Adhesion: elastocapillary coalescence in wet hair. *Nature* **432**, 690 (2004).
193. Duprat, C., Protiere, S., Beebe, A. & Stone, H. A. Wetting of flexible fibre arrays. *Nature* **482**, 510 (2012).
194. Bico, J., Reyssat, É. & Roman, B. Elastocapillarity: when surface tension deforms elastic solids. *Annu. Rev. Fluid Mech.* **50**, 629–659 (2018).
195. Vazquez, G., Alvarez, E. & Navaza, J. M. Surface tension of alcohol water. Water from 20 to 50 degrees C. *J. Chem. Eng. Data* **40**, 611–614 (1995).
196. Hell, S. W. Microscopy and its focal switch. *Nat. Meth.* **6**, 24–32 (2009).
197. Webb, R. H. Confocal optical microscopy. *Rep. Prog. Phys.* **59**, 427–471 (1996).
198. Marquet, P. et al. Digital holographic microscopy: a noninvasive contrast imaging technique allowing quantitative visualization of living cells with subwavelength axial accuracy. *Optics Lett.* **30**, 468–470 (2005).
199. Garcia-Sucerquia, J. et al. Digital in-line holographic microscopy. *Appl. Opt.* **45**, 836–850 (2006).
200. Merola, F. et al. Driving and analysis of micro-objects by digital holographic microscope in microfluidics. *Opt. Lett.* **36**, 3079–3081 (2011).
201. Wreley, S. T. & Meinhart, C. D. Recent advances in micro-particle image velocimetry. *Annu. Rev. Fluid Mech.* **42**, 557–576 (2010).
202. Versluis, M. High-speed imaging in fluids. *Exp. Fluids* **54**, 1458 (2013).
203. van der Bos, A., Zijlstra, A., Gelderblom, E. & Versluis, M. iLIF: illumination by laser-induced fluorescence for single flash imaging on a nanosecond timescale. *Exp. Fluids* **51**, 1283–1289 (2011).
204. van der Bos, A. et al. Velocity profile inside piezoacoustic inkjet droplets in flight: comparison between experiment and numerical simulation. *Phys. Rev. Appl.* **1**, 014004 (2014).
205. Switkes, M. & Ruberti, J. W. Rapid cryofixation/freeze fracture for the study of nanobubbles at solid–liquid interfaces. *Appl. Phys. Lett.* **84**, 4759–4761 (2004).
206. Schlucker, S. Surface-enhanced Raman spectroscopy: concepts and chemical applications. *Angew. Chemie Int. Ed.* **53**, 4756–4795 (2014).
207. Whitesides, G. M. The origins and the future of microfluidics. *Nature* **442**, 368–373 (2006).
208. Squires, T. & Quake, S. Microfluidics: fluid physics at the nanoliter scale. *Rev. Mod. Phys.* **77**, 977–1026 (2005).
209. Garstecki, P., Fuerstman, M. J., Stone, H. A. & Whitesides, G. M. Formation of droplets and bubbles in a microfluidic T-junction: scaling and mechanism of break-up. *Lab Chip* **6**, 437–446 (2006).
210. Eijkel, J. C. T. & van den Berg, A. Nanofluidics: what is it and what can we expect from it? *Microfluid. Nanofluidics* **1**, 249–267 (2005).
211. deMello, A. J. Control and detection of chemical reactions in microfluidic systems. *Nature* **442**, 394–402 (2006).
212. Lach, S., Yoon, S. M. & Grzybowski, B. A. Tactic, reactive, and functional droplets outside of equilibrium. *Chem. Soc. Rev.* **45**, 4766–4796 (2016).
213. Spandan, V., Lohse, D., de Tullio, M. D. & Verzico, R. A fast moving least squares approximation with adaptive Lagrangian mesh refinement for large scale immersed boundary simulations. *J. Comput. Phys.* **375**, 228–239 (2018).
214. Diddens, C. Detailed finite element method modeling of evaporating multi-component droplets. *J. Comput. Phys.* **340**, 670–687 (2017).
215. Heil, M. & Hazel, A. L. in *Fluid–Structure Interaction* (eds Schafer, M. & Bungartz, H.-J.) 19–49 (Springer, 2006).
216. Heil, M. & Hazel, A. L. Fluid–structure interaction in internal physiological flows. *Annu. Rev. Fluid Mech.* **43**, 141–162 (2011).
217. Seo, J. H. & Mittal, R. A sharp-interface immersed boundary method with improved mass conservation and reduced spurious pressure oscillations. *J. Comput. Phys.* **230**, 7347–7363 (2011).
218. Kim, J. Phase-field models for multi-component fluid flows. *Commun. Comput. Phys.* **12**, 613–661 (2012).
219. Sussman, M., Smereka, P. & Osher, S. A level set approach for computing solutions to incompressible two-phase flow. *J. Comput. Phys.* **114**, 146–159 (1994).
220. Sethian, J. A. & Smereka, P. Level set methods for fluid interfaces. *Annu. Rev. Fluid Mech.* **35**, 341–372 (2003).
221. de Langavant, C. C., Guittet, A., Theillard, M., Temprano-Coleto, F. & Gibou, F. Level-set simulations of soluble surfactant driven flows. *J. Comput. Phys.* **348**, 271–297 (2017).
222. Gibou, F., Fedkiw, R. & Osher, S. A review of level-set methods and some recent applications. *J. Comput. Phys.* **353**, 82–109 (2018).
223. Chen, S. & Doolen, G. D. Lattice Boltzmann method for fluid flows. *Annu. Rev. Fluid Mech.* **30**, 329–364 (1998).

224. Aidun, C. K. & Clausen, J. R. Lattice-Boltzmann method for complex flows. *Annu. Rev. Fluid Mech.* **42**, 439–472 (2010).
225. Perlekar, P., Benzi, R., Clercx, H. J., Nelson, D. R. & Toschi, F. Spinodal decomposition in homogeneous and isotropic turbulence. *Phys. Rev. Lett.* **112**, 014502 (2014).
226. Hessling, D., Xie, Q. & Harting, J. Diffusion dominated evaporation in multicomponent lattice Boltzmann simulations. *J. Chem. Phys.* **146**, 054111 (2017).
227. Koplik, J. & Banavar, J. R. Continuum deductions from molecular hydrodynamics. *Annu. Rev. Fluid Mech.* **27**, 257–292 (1995).
228. Frenkel, D. & Smit, B. *Understanding Molecular Simulations: From Algorithm to Applications* (Academic, 1996).
229. Lauga, E., Brenner, M. P. & Stone, H. A. in *Handbook of Experimental Fluid Dynamics* (eds Tropea, C. et al.) 1219–1240 (Springer, 2007).
230. Bocquet, L. & Charlaix, E. Nanofluidics, from bulk to interfaces. *Chem. Soc. Rev.* **39**, 1073–1095 (2010).
231. Maheshwari, S., van der Hoef, M., Zhang, X. & Lohse, D. Stability of surface nanobubbles: a molecular dynamics study. *Langmuir* **32**, 11116–11122 (2016).
232. Maheshwari, S., van der Hoef, M., Rodriguez Rodriguez, J. & Lohse, D. Leakiness of pinned neighboring surface nanobubbles induced by strong gas–surface interaction. *ACS Nano* **12**, 2603–2609 (2018).
233. Diddens, C., Li, Y. & Lohse, D. Competing Marangoni and Rayleigh convection in evaporating binary droplets. Preprint at *arXiv* <https://arxiv.org/abs/2005.14138> (2020).
234. Taylor, G. Dispersion of soluble matter in solvent flowing slowly through a tube. *Proc. R. Soc. Lond. A* **219**, 186–203 (1953).
235. Aris, R. On the dispersion of a solute in a fluid flowing through a tube. *Proc. R. Soc. Lond. A* **235**, 67–77 (1956).
236. Aris, R. On the dispersion of a solute by diffusion, convection and exchange between phases. *Proc. R. Soc. Lond. A* **252**, 538–550 (1959).
237. Anna, S. L., Bontoux, N. & Stone, H. A. Formation of dispersions using ‘flow focusing’ in microchannels. *Appl. Phys. Lett.* **82**, 364–366 (2003).
238. Utada, A. et al. Monodisperse double emulsions generated from a microcapillary device. *Science* **308**, 537–541 (2005).
239. Solans, C., Morales, D. & Homs, M. Spontaneous emulsification. *Curr. Opin. Colloid Interface Sci.* **22**, 88–93 (2016).

Acknowledgements

We thank our colleagues, postdocs, PhD students and other students for their contributions to our understanding of physicochemical hydrodynamics of droplets and for the intellectual stimulation we have enjoyed when doing physics together. In the context of the subjects covered here, we thank L. Bao, K. Leong Chong, P. Kant, Z. Lu, A. Prosperetti, V. Spandan,

M. Versluis, C.-W. Visser, H. Wijshoff, H. Yu and in particular C. Diddens, Yanshen Li, Yaxing Li and H. Tan. We also thank A. Juel, S. Karpitschka, C. Maas, A. Prosperetti, J. Snoeijer and H. Stone for comments on the manuscript. D.L. thanks D. van Gils for drawing many figures and acknowledges support from the Dutch Research Council (NWO) under several projects, from the ERC Advanced Grant “DDD” under the project number 740479, and from the ERC Proof-of-Concept Grant “NanoEX” under the project number 862032. X.H.Z. acknowledges support from the Natural Science and Engineering Council of Canada (NSERC) and from the Canada Research Chairs programme.

Author contributions

Both authors contributed to all aspects of manuscript preparation, revision and editing.

Competing interests

The authors declare no competing interests.

Publisher’s note

Springer Nature remains neutral with regard to jurisdictional claims in published maps and institutional affiliations.

Reviewer information

Nature Reviews Physics thanks C. Misbah and the other, anonymous, reviewer(s) for their contribution to the peer review of this work.

© Springer Nature Limited 2020